University of Arkansas, Fayetteville

ScholarWorks@UARK

Graduate Theses and Dissertations

12-2021

Mission Profile Effects on Automotive Drivetrain Electronics Reliability: Modeling and Mitigation

Bakhtiyar Mohammad Nafis
University of Arkansas, Fayetteville

Follow this and additional works at: https://scholarworks.uark.edu/etd

Part of the Applied Mechanics Commons, Computer-Aided Engineering and Design Commons, Electro-Mechanical Systems Commons, and the Power and Energy Commons

Citation

Mohammad Nafis, B. (2021). Mission Profile Effects on Automotive Drivetrain Electronics Reliability: Modeling and Mitigation. *Graduate Theses and Dissertations* Retrieved from https://scholarworks.uark.edu/etd/4340

This Thesis is brought to you for free and open access by ScholarWorks@UARK. It has been accepted for inclusion in Graduate Theses and Dissertations by an authorized administrator of ScholarWorks@UARK. For more information, please contact scholar@uark.edu, uarepos@uark.edu.

Mission Profile Effects on Automotive Drivetrain Electronics Reliability:
Modeling and Mitigation

A thesis submitted in partial fulfillment
of the requirements for the degree of
Master of Science in Mechanical Engineering

by

Bakhtiyar Mohammad Nafis
Bangladesh University of Engineering and Technology
Bachelor of Science in Mechanical Engineering, 2017

December 2021
University of Arkansas

This thesis is approved for recommendation to the Graduate Council.

David Huitink, Ph.D.
Thesis Director

Xiangbo Meng, Ph.D.
Committee Member

Morgan Ware, Ph.D.
Committee Member

Abstract

The reliability of electronic devices is dependent upon the conditions to which they are subject. Temperature variations coupled with differences in thermal expansion between bonded materials results in thermomechanical stresses to build up, which can instigate failure in the interconnects or other critical regions. With the move towards electrification in the automotive industry, there is the increasingly important consideration of powertrain electronics reliability, the pertinent conditions being governed by the drive cycle or mission profile of the vehicle. The mission profile determines the power dissipated by the electronic devices, which determines the peak and mean temperature, temperature swing and the resultant stress range, as well the effective thermal cycling frequency. This thesis, submitted in partial completion of the requirements for the Master of Science in Mechanical Engineering, herein investigates the relationship between predicted lifetime of electronic components in the drivetrain of an electric or hybrid electric vehicle and the mission profile it is operated at. The primary datasets are taken from the Environment Protection Agency (EPA) fuel economy test cycles, which lists various standard mission profiles for different driving conditions. The thermal profiles resulting from each mission profile are used to extract damage parameters and used to estimate time to failure. As the lifetimes are dependent on the thermal transients, ways are explored to minimize the temperature swings. One such way is to use phase change materials as thermal reservoirs that can be very effective thermal management option under the right conditions. Phase change materials absorb thermal energy as latent heat, which allows them to absorb a very large amount of heat per unit volume, but they are limited by low thermal conduction and long regeneration times. An affordable and widely available phase change material, paraffin, is used as a case study. A model is developed to mimic a widely available commercial power module, and detailed parametric studies are done to understand the

effectiveness and best practices in using paraffin as a phase change material in cooling. The results show that PCMs hold great potential in automotive electronics cooling, but there is a delicate trade-off between the latent heat, thermal conductivity, and dissipated power that can be handled. As coefficient of heat transfer of secondary cooling mechanism gets larger, using PCMs become less advantageous.

©2021 by Bakhtiyar Mohammad Nafis
All Rights Reserved

Acknowledgements

First of all, I would like to thank my parents, Dr. Sayeda Parveen Akhtar and Md. Matiur Rahman, for their love and for instilling in me the value of education and service, and without them I would not be here today. I would also like to thank my sister, Feiroz, for her lifelong friendship and love.

I would like to thank my graduate advisor, Dr. David Huitink for his mentorship, and for keeping faith in me through thick and thin. He has been a constant source of knowledge and expertise and has provided me invaluable guidance, both as a research adviser and teacher. I would also like to thank my committee members, Dr. Morgan Ware and Dr. Xiangbo Meng for their assistance and guidance.

Along with my advisory committee, I would like to thank my friends and fellow co-workers in the EMPIRE Lab who have offered assistance in taking measurements and been there for me to discuss ideas, especially Hayden Carlton, Cody Marbut, Mahsa Montazeri, Reece Whitt, Joshua Tompkins, Ange Iradukunda, Tumi Olatunji, Alexis Krone, John Harris, Dustin Pense, Joshua Kasitz, Alicia Medina Garcia, Collin Ruby and Joshua Pennington.

Throughout the process of carrying out the work that are included in this thesis, I have had the opportunity to work with many fantastic engineers, scientists, and graduate students. Thank you Dr. Alan Mantooth and his team at the Department of Electrical Engineering at the University of Arkansas, Dr. Yue Zhao and his students Zhongjing Wang, Mohammad Hazzaz Mahmud and Yuheng Wu, Dr. Nenad Miljkovic and Md. Jahid ul Haque from the University of Illinois, Urbana-Champagne, and Dr. Chris Farnell and Justin Jackson of the National Center for Reliable Electric Power Transmission (NCREPT).

I would also like to thank the administrative staff in the Mechanical Engineering department, specifically Brenda Bunch, Phyllis Dranger, and Melynda Hart. I very much appreciate your help with all of my equipment orders, travel assistance, and academic advising over the past couple of years.

I would like to give big thanks Mr. Ben Fleming who is always there to help with any fabrication or machining need.

And finally, I would like to thank my wife, Mackenzie. Thank you, for always being there for me, for your continual support, for your words of encouragement, and for making the amazing meals while I was trying to wrap this thing up. I love you.

Table Of Contents

1. Introduction to Reliability Assessment of Automotive Electronics 1

1.1 Typical Failure Mechanisms in Power Electronics 4

1.2 Modeling Power Electronics Reliability 8

1.3 Summary of Electronics Reliability Assessment in Automotive Electronics..................... 11

1.4 Motivation and Objectives of Present Research Effort.. 12

1.5 References.. 13

2. Rainflow Counting Algorithms for Damage Quantification in Automotive Electronics 18

2.1 Brief Introduction to Rainflow and Range Counting.. 20

2.2 Rainflow Counting in Life Prediction of Electronics 22

2.2 Summary and Conclusion 25

2.3 References.. 25

3. Development of Mission Profile Dependeent High-Fidelity Thermal Behavior Modeling Tool for Electric Drivetrains 28

3.1 First Pass Analysis 31

3.2 Second Pass Analysis: Lumped Capacitance Thermal Circuit Model............................... 37

3.3 Testing and Validation of Model 39

3.4 Summary 41

3.5 References 42

4. Rainflow Counting and Damage Accummulation due to Thermal Transients 43

4.1 Temperature Profile Estimation 45

4.2 Drive Schedules Applied to LC Model: Mean Temperatures, Temperature Swings, Effective Frequencies 48

4.3 Reliability Models and Drive Schedules Compared 49

4.3.1 Thermal Characteristics During Startup 51

4.3.2 Thermal Characteristics During Continuous Operation 52

4.3.3 Reliability Assessment and Comparison 54

4.3.4 Characterizing Effective Frequency and Effect on Reliability and Computational Effort 55

4.4. Summary and Conclusions 59

4.5. References 60

5. System Level Thermal Management and Reliability of Automotive Electronics: Goals and Opportunities using Phase Change Materials 62

5.1.Abstract 62

5.2. Introduction 63

5.3. Computational Method and FEA Validation 66

5.4. Results and Discussions 72

5.5. Reliability Consideration 75

5.6. Implication for Cooling System Design 76

5.7. Conclusion 80

5.8. Acknowledgement 81

5.9. References 82

6 Conclusions 86

6.1 Summary 86

6.2 Significance and Future Opportunities 89

Appendix 91

Appendix A1: Example Calculation of Motor Power from Drive Schedule 91

Appendix A2: Thermal and Reliability Modeling Computer Program 93

Appendix A3: Vitae 97

LIST OF PUBLISHED PAPERS

1. Chapter 5: Nafis, B. M., Iradukunda, A. C., and Huitink, D., 2020, " System-Level Thermal Management and Reliability of Automotive Electronics: Goals and Opportunities Using Phase-Change Materials," Journal of Electronic Packaging, 142(4), 041108.

Chapter 1. Introduction to Reliability Assessment of Automotive Electronics

Power electronics are the solid-state devices that are used to convert and control electric power. As hybrid and electric vehicles become more common, the priorities of automotive electronics have changed to include more power electronics in the drivetrain. The main function of the power electronics in the drivetrain is to convert the direct current (DC) output from the battery into alternating current (AC) that is then fed into the electric motor. The main component in such as drivetrain is the inverter, which occupies a place between the energy storage (battery) and the motor(s). In hybrid vehicles the battery-inverter-motor system works in conjunction with the conventional powertrain, but in electric vehicles they usually work as standalone systems. Figure 1 illustrates the fundamental characteristics of a hybrid and electric drivetrain.

The power electronics that are part of a vehicle's drivetrain are subject to different demands than the entertainment or comfort-focused electronic components. The stresses that an automotive electronic system will be subject to arise from three factors.

i) Electrical loading: Drivetrain electronics tend to handle much larger voltages and currents than an infotainment system. Table 1 highlights the voltage levels of some key components in hybrid and electric passenger vehicles.

Table 1. Voltage levels (in Volts) of various components in passenger vehicles [1]

Components	Mild Hybrid	Full/Plug-in Hybrid	EV
Electric Motor	12-120	250-300	300/600
Inverter (DC/AC)	15-200	400-420	400/420/800
Battery	15-200	400-420	400/420/800

ii) Mechanical vibration: Drivetrain power electronics are more likely to be in closer proximity to the motor or engine

iii) Environmental conditions: Drivetrain power electronics are more likely to be exposed to extreme conditions, such as high or low ambient temperatures, moisture etc.

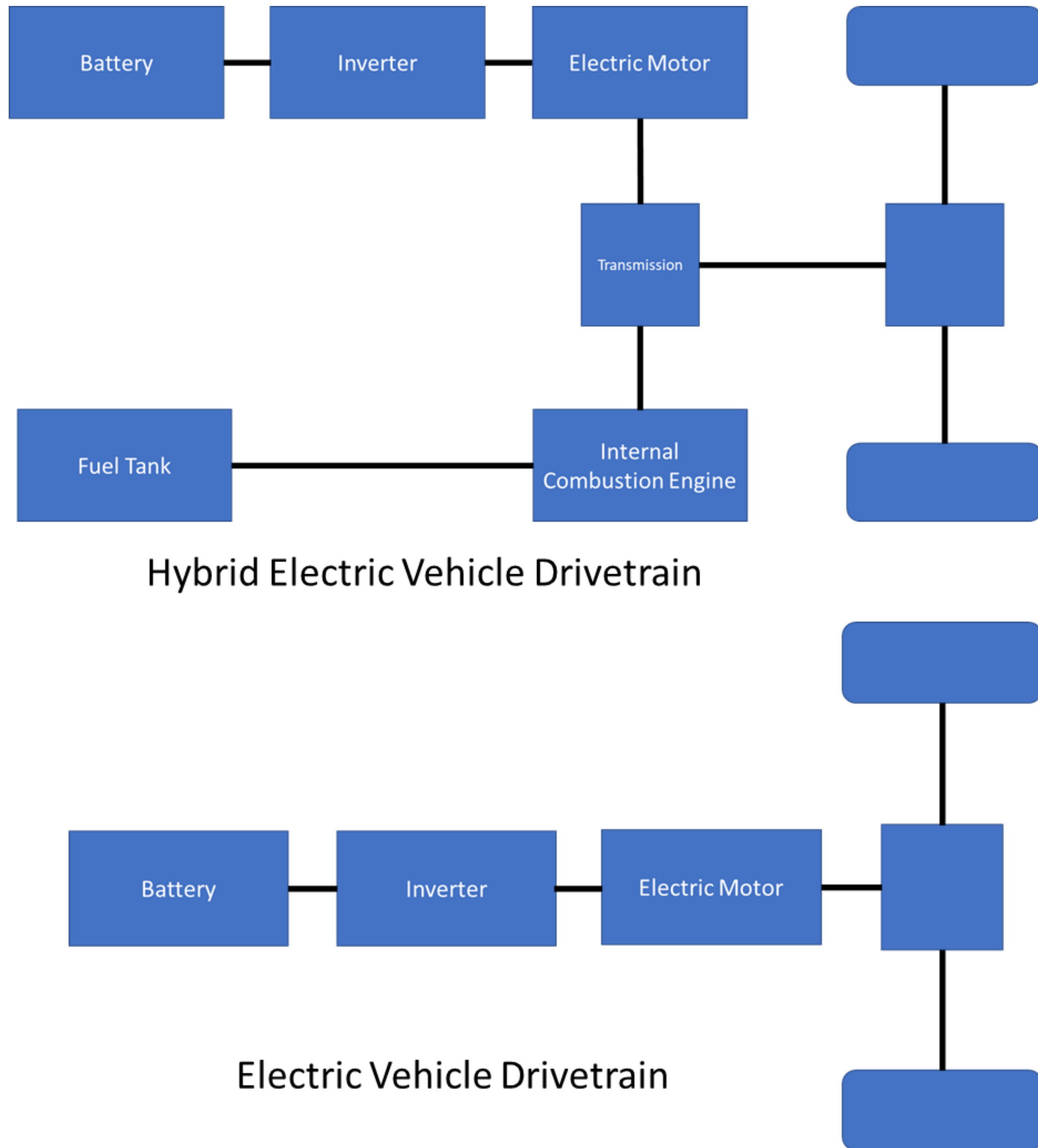

Figure 1. Illustration of hybrid and electric vehicle drivetrains

A powertrain electronic device may be subject to continuous temperature swings. In a study on traction drives for an urban tram, it was found that temperature swings up to 80 C and power cycles between 10^6 and 10^8 are to be expected [2]. Figure 2 shows the temperature profile for a hybrid vehicle, showing numerous small thermal cycles [3]. The smaller temperature swings would be less damaging per cycle, but a high effective frequency resulting in higher number of cycles can also have reliability considerations as they will also contribute to loss of expected life.

Due to these recent changes, automotive electronics reliability is becoming a more critical factor when it comes to the entire vehicle system, and therefore it is becoming more important to understand the underlying mechanisms that lead to failure. They will be discussed later in this chapter.

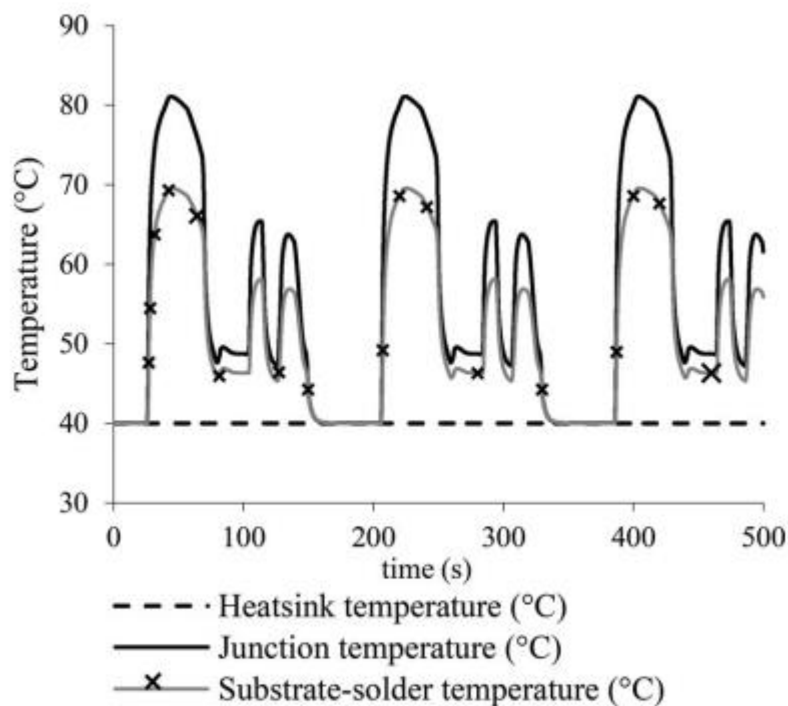

Figure 2. Example of a temperature profile of the components of a power inverter [3] © IEEE 2015

Figure 3 gives the relative distribution of failing components in power electronic systems [4]. Even though the information is from 2007, it does show the reliability limiting role of several different failure areas. For example, capacitors often limit the reliability of a system, while solder interconnects are the most likely failure point in packaging.

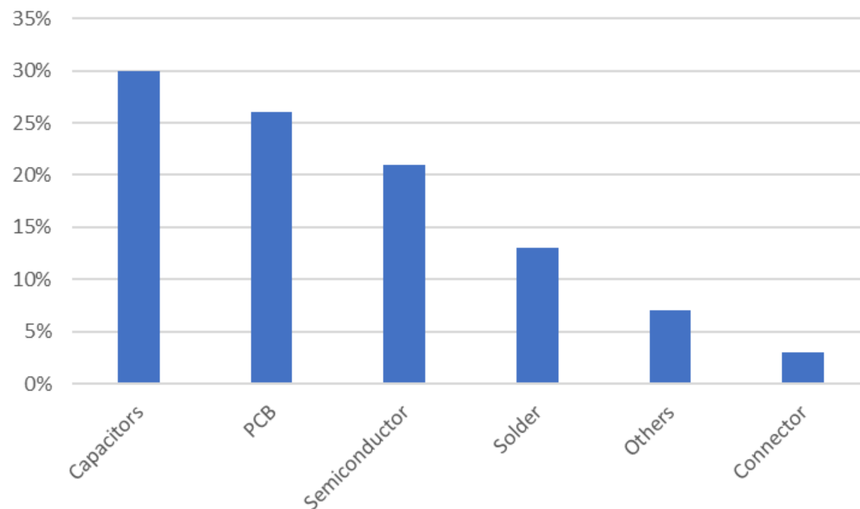

Figure 3. Failure distribution ranking [4]

1.1 Typical Failure Mechanisms in Power Electronics

The failure mechanisms in electrical or electronic devices can be classified into three types.

I) System level failure: This is what happens when the system stops operating as designed. The system is a complex combination of various components or subsystems working together. Failure of a certain component may or may not result in the entire system failing, as that would depend on the exact role the component plays and the number of occurrences of such failure.

II) Component related failure mechanism: This is the failure of a component to operate as intended. This can be further divided into device failure and packaging failure.

a. Device failure: This category includes the failure of a device to perform its core operation, and is not related to the failure of its connections (which are categorized as packaging failure). For example, voltages and currents that are too high can result in electrical overstress in semiconductor dies [5, 6]. Electrostatic discharge can cause failure by destroying the integrity of the gate oxide layer. This can happen when excessive gate voltage is applied without sufficient protection [7]. Electromigration can happen in the conductors due to electromotive force or interdiffusion [8, 9]. Thermally activated degradation mechanisms are also common, as almost all silicon devices are subject to high temperature degradation [10]. In capacitors, high voltage stresses can cause temperature-induced degradation to accelerate [11, 12]. All of these are examples of the core functionality of the device being disrupted.

b. Packaging failure: These are failure that have to do with how the devices or components are to interact with other devices and its surroundings. Packaging failures are the most common types of failure in electronics, with the possible exception of capacitor device failure. They are primarily driven by differences in the coefficients of thermal expansion (CTE) between adjacent materials. When there is a temperature swing, adjacent materials expand at different rates. This causes stresses and strains to build up. Repeated temperature swings can cause fatigue in the materials.

The most likely location of packaging failure are the interconnects and die attach. As the two main types of interconnects are bond wires and solder bumps, they are discussed below.

i. Bond wire liftoff: Mismatches in coefficients of thermal expansion results in crack growth in the interface between the bond wire, usually (but not exclusively) aluminum, and the chip, typically made of patterned silicon [2, 13, 14]. There is a temperature induced strain at the interface, which lead to stresses being developed. Repeated temperature swings effectively cause stress cycles. This leads to initiation and propagation of cracks. This degrades the performance of the bond wire and increases electrical and thermal resistance. When the crack extends the entirety of the interface, the bond wire lifts off completely [15-18]. In case of very large temperature swings, cracks may propagate from multiple directions, hence accelerating the failure mechanism significantly. However, in some cases annealing has also been observed, which slows down the failure process [19, 20].

ii. Solder fatigue: This is the damage accumulation in solder interconnects or die attach due to repeated stress-strain cycles resulting from repeated temperature swings [21, 22]. They are influenced by the initial solder microstructure, metallization of the material being bonded, as well as any intermetallic compound that forms [23 – 25]. Due to mismatches CTE, voids form at the interfaces. These voids reduce the effective area for heat to escape by conduction from the die, which in turn makes the die become hotter, and the process accelerates as the voids grow [26, 27]. The increased thermal resistance can cause severe localized heating of die attach and can

damage the chip [28, 29]. In some cases, when the power cycling of the power electronic device results in thermal cycling of the materials, the result is strain cycling and induced stress cycling in the solder. The crack length in the solder increases with the number of cycles and at one point, the crack growth rate increases with the hysteresis area in the stress-strain plot.

There are a number of other packaging related failures that have been observed in power electronics, but the focus of this study will remain on the two discussed above, as they are the most common and typically are the first to occur. Table 2 summarizes the most common failures, their stressors and importance levels. Figure 4 shows the two most common types of interconnect failures: wire bond liftoff and solder joint cracking.

Table 2. Different failure areas, their stressors and significance of stressor in causing failure (4 being most significant) [30]

Stressors	Die	Capacitor	Interconnects	
			Wirebond	Solder Joint
Temperature swing ΔT	4	0	4	4
Average Temperature T	3	2	3	3
dT/dt	1	1	1	0
Relative Humidity	1	3	1	1

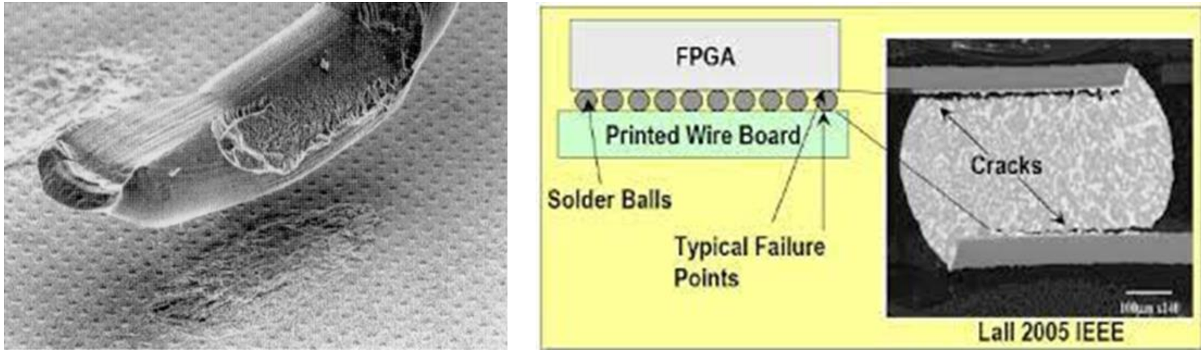

Figure 4. Aluminum bond wire heel cracking (left, [31] © 2010 IEEE) and solder joint cracking (right, [32] © 2008 IEEE)

1.2 Modeling Power Electronics Reliability

With the knowledge of failure mechanisms, reliability models of power device packaging can be built to facilitate failure analysis, lifetime prediction and condition monitoring. Developing such a model is usually a two-step process that requires detailed information about the geometry and materials, failure rate and distributions, as well as physics of failure information.

Step 1. Electrothermal modeling of the device chip and packaging during a loading period, generating the temperatures throughout the duration loading period. Thermal models can be of different types. The most accurate model of this type use the finite element approach, but those can be limited due to computational expense and time required, especially if a simpler model is sufficient [33, 34]. Thermal equivalent networks are frequently used in electrothermal modeling of converters, and may be used easily in circuit simulators. Foster or Cauer networks are used to represent the thermal diffusion in the packaging [35 - 38]. Figure 5 (a) and (b) illustrate examples of Foster and Cauer thermal networks.

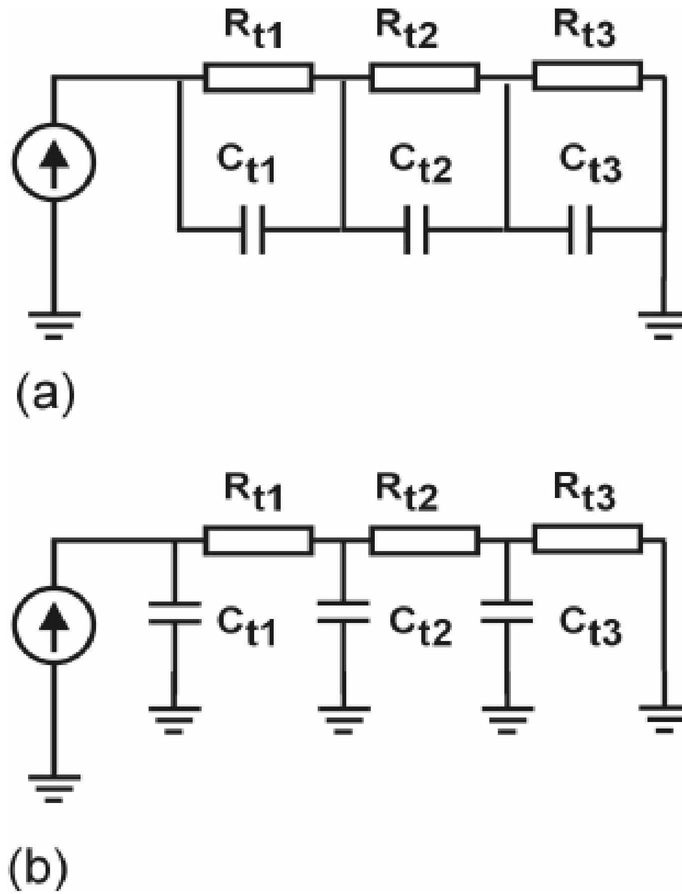

Figure 5. (a) Foster and (b) Cauer thermal networks where R and C represents thermal resistance and capacitance, respectively and the current source represents the heat flux

Step 2. Thermomechanical modeling of the packaging materials, predicting the accumulated damage and remaining life, based on input from the electrothermal model. This requires detailed information such as physics of failure models, empirical correlation, failure distribution data, time history of loading, to name a few, depending on the focus and detail required for the purpose. The aim is to capture the failure mechanism itself, and historically, the focus has been on bond wire liftoff and solder cracking. The bond wire liftoff mechanism is thermally activated, and can be expressed as an Arrhenius correlation

$$N_f = A\, \Delta T^{\alpha} \exp\left(\frac{E_A}{RT_m}\right) \tag{1}$$

Where α and A are constants depending on material, T_m is the mean temperature (kelvin) during cycling, ΔT is the temperature swing, E_A is the activation energy and R is the gas constant. A more detailed model for describing crack propagation under fatigue conditions can also be used according to the Paris law [39].

$$\frac{da}{dN} = C\,\Delta K^m \tag{2}$$

where a is the crack length (in meters), N is the number of load cycles, C and m are material constants, and ΔK is the range of the stress intensity factor [40].

Most reliability testing are done for one of two purposes: qualification, and lot disposition. In both these types of testing, the failures are accelerated many times their expected rate during operation. Qualification testing is often done on a product to provide a reliability benchmark that allows it to be used with confidence for certain time duration. It is often required by users and are subject to industry and regulatory standards. Accelerated testing is also done on lots to assess their reliability. Usually, the acceleration is higher as the aim is often to achieve failure which can then be analyzed and addressed. The acceleration factor (AF) is the quantity that expresses the level of acceleration that is applied. It is the ratio of life at use conditions to the life at test conditions.

For solder, Coffin-Manson expressions are widely used to model lifetimes associated with fatigue failure. For solder and wirebond interconnections, the most widely used model to describe acceleration of failure in a temperature cycling environment is given as the Norris-Landzberg expression below.

$$AF = \frac{N_O}{N_t} = \left(\frac{f_t}{f_O}\right)^a \left(\frac{\Delta T_t}{\Delta T_O}\right)^b \exp\left[\frac{E_a}{R}\left(\frac{1}{T_{max,O}} - \frac{1}{T_{max,t}}\right)\right] \tag{3}$$

Here *AF* stands for acceleration factor, *N* stands for cycles to failure, E_a is the activation energy and *a* and *b* are exponents of frequency and temperature swing, respectively. The subscripts *t* and *O* correspond to test and operational conditions. There are more detailed models for solder degradation as well, but Coffin-Manson expressions are widely used due to their simplicity and ease of use.

1.3 Summary of Electronics Reliability Assessment in Automotive Electronics

Due to electrification, the components that go into a car's powertrain are changing. Power electronics are now critical components of the drivetrain. As electric drivetrains become more common, their reliability is becoming more important. The key challenge, however, lies in the fact that the drivetrain power electronics are being subject to high stress values. They have to be able to handle large power loads and correspondingly large voltages and currents. The power loads give rise to heat dissipation in the power electronics semiconductors and the resultant temperature fluctuations are the key drivers of failure in electronic devices. The electronic devices are limited by their most vulnerable area, and in electronic packaging, the interconnects are usually the first to fail. The most widely adopted interconnect technology, solder and bond wires, are subject to damage and failure due to fluctuating temperatures.

Different types of models have been developed to simulate thermal behavior of automotive electronics and to quantify their reliability. The simpler ones are empirical correlations that relate the degradation and life to external parameters. Examples of such approach would be an Arrhenius relationship that relates bond wire lifetime to the temperature swing and other geometry and material-specific factors. More detailed models have also been developed, but they are only useful when the exact packaging structure is known. Crack initiation and propagation is complicated and nearly all such models and equations require distributed parameters, such as stress, which is

dependent on geometry, material, and load levels. This problem can be solved by the aid of Finite Element Method (FEM), which requires lengthy simulation to calculate the thermomechanical behavior.

1.4 Motivation and Objectives of Present Research Effort

It is said that automotive electronics reliability testing and assessment starts and ends with the mission profile. The driving conditions and characteristics are the critical factors that help decides a component's lifetime. However, there remain challenges involved in effectively modeling and mitigating the effects of a vehicle's mission profile. For this purpose, finite element modeling is used, but it involves from long and expensive computation process that makes it unsuitable for real time health monitoring. On the other hand, there are empirical correlations that have been developed for most critical failure mechanisms in electronics, but they require a thermal model that is input and are most accurate when they are provided the parameter specific to the geometry and materials in question.

Another challenge in automotive electronics is the mitigation of the effects of mission profiles. The frequent temperature swings are key factors in damage and shorten the lifetime of electronic components and minimizing them is key in lengthening useful life of electronics.

The key objectives of this work can be broken down in the following way:

1. To develop a modeling tool to effectively translate the effects of a vehicle's mission profile to the electronics component level. The model must demonstrate a sufficient level of accuracy as well as ease of computation.
2. Optimize the approach for reliability computation based on the model to find the right tradeoff between accuracy and computational time.

3. To demonstrate the use of phase change materials as a way of mitigating the temperature swings in automotive powertrains.
4. To identify the conditions under which using phase change materials is most useful.

The next chapters will outline the activity towards achieving the objectives. Chapter 2 will introduce rainflow counting as a tool of quantifying accumulated damage in reliability assessment of mission profile-based situations. Chapter 3 will describe the process of model development that is a tradeoff between accuracy and ease of use. Chapter 4 describes the application of the model in conjunction with a rainflow counting algorithm to compute predicted reliability and carry out optimization to minimize computational time while still maintaining sufficient stability. Chapter 5 describes in detail the effort to minimize the temperature swings in automotive power electronics temperature profiles using phase change materials. An envelope is presented to act as a blueprint for PCM integration in automotive power modules. Chapter 6 provides a summary of the findings and discusses the path forward.

1.5 References

1. ZVEI-German, and Electronic Manufacturers Association, "Voltage classes for electric mobility." *Frankfurt am Main, Germany* (2013).

2. M. Held, P. Jacob, G. Nicoletti, P. Scacco, and M. H. Poech, “Fast power cycling test of IGBT modules in traction application,” in Proc. Int. Conf. Power Electron. Drive Syst., 1997, pp. 425–430.

3. Musallam, Mahera, et al. "Mission profile-based reliability design and real-time life consumption estimation in power electronics." *IEEE Transactions on Power Electronics* 30.5 (2014): 2601-2613.E. Wolfgang, “Examples for failures in power electronics systems,” presented at ECPE Tutorial ‘Rel. Power Electron. Syst.’, Nuremberg, Germany, Apr. 2007.

4. Voldman, Steven H. "System and Component Failure from Electrical Overstress and Electrostatic Discharge." *System of System Failures* (2018): 9.

5. Mazza, B., et al. "Electrical overstress effect characterization on Power MOS Trenchfet and correlation with time dependent dielectric breakdown." *Microelectronics Reliability* 125 (2021): 114351.

6. C. Duvvury, J. Rodriguez, C. Jones, and M. Smayling, “Device integration for ESD robustness of high voltage power MOSFETs,” in Proc. Int. Electron Devices Meeting, 1994, pp. 407–411.

7. Lienig, Jens, and Matthias Thiele. *Fundamentals of Electromigration-Aware Integrated Circuit Design*. Springer, 2018.

8. Zhang, Peng, Songbai Xue, and Jianhao Wang. "New challenges of miniaturization of electronic devices: Electromigration and thermomigration in lead-free solder joints." *Materials & Design* 192 (2020): 108726.

9. D. A. Grant and J. Gowar, Power MOSFET-Theory and Applications. New York: Wiley, 1989.

10. Gupta, Anunay, et al. "A review of degradation behavior and modeling of capacitors." *International Electronic Packaging Technical Conference and Exhibition*. Vol. 51920. American Society of Mechanical Engineers, 2018.

11. Hui, Li, et al. "Reliability modelling and analysis on MMC for VSC-HVDC by considering the press-pack IGBT and capacitors failure." The Journal of Engineering 2019.16 (2019): 2219-2223.

12. Luo, Yihua. "Identification and predictive modeling of high propensity of defects and field failure in copper-aluminum wire bond interconnect under exposure to high temperature and humidity." (2018).

13. Lall, Pradeep, et al. "Measurement of Ion-Mobility in Copper-Aluminum Wirebond Electronics Under Operation at High Voltage and High Temperature." *International Electronic Packaging Technical Conference and Exhibition*. Vol. 58097. American Society of Mechanical Engineers, 2017.

14. M. Ciappa and W. Fichtner, “Lifetime prediction of IGBT modules for traction applications,” in Proc. IEEE Int. Rel. Phys. Symp., 2000, pp. 210– 216.

15. Eivani, A. R., H. R. Mirzakoochakshirazi, and H. R. Jafarian. "Investigation of joint interface and cracking mechanism of thick cladding of copper on aluminum by equal channel angular pressing (ECAP)." *Journal of Materials Research and Technology* 9.3 (2020): 3394-3405.

16. Jiang, Maogong, et al. "Finite element modeling of igbt modules to explore the correlation between electric parameters and damage in bond wires." *2019 IEEE Energy Conversion Congress and Exposition (ECCE)*. IEEE, 2019.

17. Hu, Keting, et al. "Cost-effective prognostics of IGBT bond wires with consideration of temperature swing." *IEEE Transactions on Power Electronics* 35.7 (2019): 6773-6784.

18. P. A. Agyakwa, W. S. Loh, M. R. Corfield, E. Liotti, S. C. Hogg, and C. M. Johnson, “Anomalous reliability behaviour of 99.99% and 99.999% pure aluminium wire bonds under thermal cycling,” in Proc. IMAPS 41st Int. Symp. Microelectron., 2008.

19. Jahangiri, Mohammadreza, et al. "Effect of annealing method and applied stress on aging behavior of copper-aluminum bimetals." *Journal of Alloys and Compounds* 816 (2020): 152676.

20. Su, Sinan, et al. "A state-of-the-art review of fatigue life prediction models for solder joint." *Journal of Electronic Packaging* 141.4 (2019): 040802.

21. Wei, Hsiu-Ping, et al. "Prediction of statistical distribution of vibration-induced solder fatigue failure considering intrinsic variations of mechanical properties of anisotropic Sn-Rich solder alloys." *2018 IEEE 68th Electronic Components and Technology Conference (ECTC)*. IEEE, 2018.

22. J. M. Thebaud, E. Woirgard, C. Zardini, and K. H. Sommer, “Extensive ´ fatigue investigation of solder joints in IGBT high power modules,” in Proc. Electron. Compon. Technol. Conf., 2000, pp. 1436–1442.

23. J. Lau, Solder Joint Reliability: Theory and Applications, 1st ed. Norwell, MA: Kluwer, 1991.

24. Anuar, Rabiatul Adawiyah Mohamed, and Saliza Azlina Osman. "The formation of intermetallic layer structure of SAC405/Cu and SAC405/ENImAg solder joint interfaces." *Soldering & Surface Mount Technology* (2020).

25. M. Ciappa, “Reliability of high-power IGBT modules for traction applications,” in Proc. IEEE Int. Rel. Phys. Symp., 2007, pp. 480–485.

26. W. Koziarz and D. Gilmour, “Anomalous thermal conductivity in regions of non-uniform die attachintegrity,” in Proc. IEEE Int. Rel. Phys. Symp., 1995, pp. 107–111.

27. D. Katsis and J. van Wyk, “Void-induced thermal impedance in power semiconductor modules: Some transient temperature effects,” IEEE Trans. Ind. Appl., vol. 39, no. 5, pp. 1239–1246, Sep./Oct. 2003.

28. Katsis and van Wyk, “A thermal, mechanical, and electrical study of voiding in the solder die-attach of power MOSFETs,” IEEE Trans. Compon. Packag. Technol., vol. 29, no. 1, pp. 127–136, Mar. 2006.

29. Wang, Huai, et al. "Transitioning to physics-of-failure as a reliability driver in power electronics." *IEEE Journal of Emerging and Selected Topics in Power Electronics* 2.1 (2013): 97-114.

30. Yang, Shaoyong, et al. "Condition monitoring for device reliability in power electronic converters: A review." *IEEE transactions on power electronics* 25.11 (2010): 2734-2752.

31. Hofmeister, James P., et al. "Ball grid array (BGA) solder joint intermittency detection: SJ BIST." *2008 IEEE Aerospace Conference*. IEEE, 2008.M. Ciappa, “Lifetime prediction on the base of mission profiles,” Microelectron. Rel., vol. 45, no. 9–11, pp. 1293–1298, 2005.

32. Jayesh, S., and Jacob Elias. "Finite element modeling and random vibration analysis of BGA electronic package soldered using lead free solder alloy− Sn-1Cu-1Ni-1Ag." *International Journal for Simulation and Multidisciplinary Design Optimization* 10 (2019): A11.

33. Alavi, Omid, Mohammad Abdollah, and Abbas Hooshmand Viki. "Assessment of thermal network models for estimating IGBT junction temperature of a buck converter." *2017 8th Power Electronics, Drive Systems & Technologies Conference (PEDSTC)*. IEEE, 2017.

34. Smirnov, Vitaliy I., et al. "Modulation method for measuring thermal impedance components of semiconductor devices." *Microelectronics Reliability* 80 (2018): 205-212.

35. Li, Jinyuan, et al. "Study on the Cauer Thermal Network Model of Press Pack IGBTs." *IOP Conference Series: Materials Science and Engineering*. Vol. 439. No. 5. IOP Publishing, 2018.

36. An, Ning, et al. "A high-precision adaptive thermal network model for monitoring of temperature variations in insulated gate bipolar transistor (IGBT) modules." *Energies* 11.3 (2018): 595.

37. P. Paris and F. Erdogan, "A critical analysis of crack propagation laws," Trans. ASME Ser D, J. Basic Eng., vol. 85, no. 4, pp. 528–534, Dec. 1963

38. R. Sundararajan, P. McCluskey, and S. Azarm, "Semi-analytic model for thermal fatigue failure for die attach in power electronic building blocks," in Proc. 4th High Temperature Electron. Conf., 1998, pp. 94–102

Chapter 2. Rainflow Counting Algorithms for Damage Quantification in Automotive Electronics

In the previous chapter, the thesis outline and objectives were laid out, a big part of which involve counting algorithms. The counting algorithms play the critical function of reducing complex loading histories, with variable amplitudes, into discrete, simple, constant amplitude loading events. In this work, counting algorithms, in particular a variant known as range counting method, will be utilized in conjunction with the Miner's Rule, an empirical model, to determine consumed or exhausted life of electronic devices. The loading histories will be the predicted temperature profiles of the power electronic devices that will be translated from the mission profiles. That process will be outlined in Chapter 3.

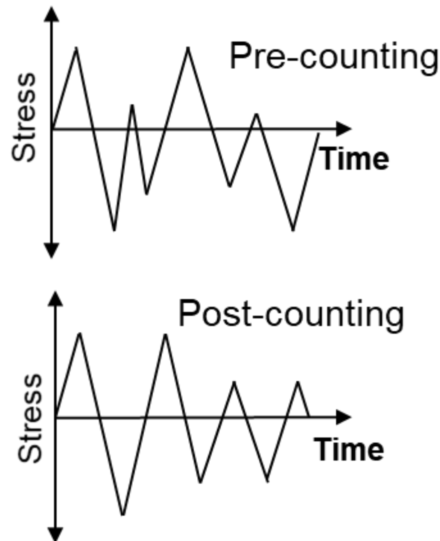

Figure 6. Load history rearrangement through cycle counting

Methods of cycle counting have been used in different applications in mechanics and reliability, especially applications relating to random load exertions, primarily in the study of fatigue damage.

Such counting methods include, but are not limited to, level crossing counting, peak counting, range counting and rainflow counting method. These methods are useful because they reduce a range of varying load into a series of simple cycles of discrete amplitudes, as shown in Fig. 6. In this figure, the cycles pre-count are random, with varying amplitudes. Post-counting, they are ordered and ready for further processing and analysis. The most obvious benefit they offer is that they enable the application of Miner's rule [1] to assess the fatigue life of a structure subject to complex non-uniform loading.

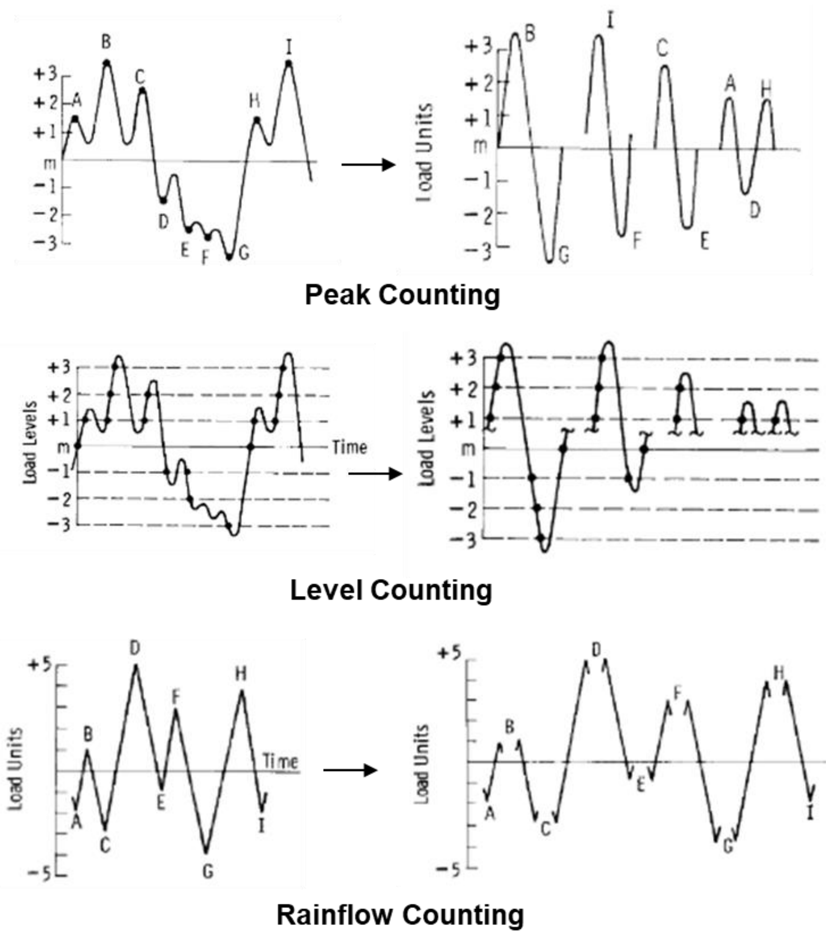

Figure 7. Peak counting, level counting and rainflow counting methods illustrated [2]

The various counting methods differ in how they count the cycles (Fig. 7). In both peak and level counting methods, discrete intervals and a reference level are created for the loading. In level counting method, counts are recorded each time a positively sloped portion of history is at or above the reference, or a negatively sloped portion is below the reference. In peak counting method, a count is recorded each time the load curve changes slope. Counts are then combined to form completed cycles using the largest cycle first.

Rainflow counting reduces the range of stresses (or load history) to a simple set of stress reversals by identifying closed hysteresis loops. Range counting is a simplified form of the method where the cycles are formed from the peaks and valleys. Consecutive peak and valley forms a half-cycle, and are then used to create a full cycle. Rainflow and range counting will be further discussed in the next section.

2.1 Brief Introduction to Rainflow and Range Counting

The counting approach to fatigue analysis was first proposed by Matsuishi and Endo in 1968 [3] to count the cycles or the half cycles of strain-time signals for structures under non-uniform loading. Matsushi and Endo's approach was based on the stress-strain behavior of the particular material (Fig. 8). It combines load reversals in a way that defines a cycle as a closed hysteresis loop, and each closed hysteresis loop i.e. a full cycle, has a strain range and mean stress associated with it that can be compared with the constant amplitude.

The counting principle is described as follows. Referring to Fig. 8, as the material deforms from point *i* to *ii*, it follows a path described by the cyclic stress-strain curve. At point *ii*, where the load is reversed, the material elastically unloads to point *iii*. When the load is exerted again from *iii* to *iv*, the material elastically deforms to point *ii*, where the material remembers its prior history of

deformation from *i* to *ii*, and deformation continues along path a to *iv* and completely disregarding event *ii* – *iii*.

Counting algorithms initially found use in structural engineering and mechanical vibration applications with arbitrary loading [4, 5]. Counting algorithms have been utilized for fatigue analysis since the 1970s. Some of the early examples of such work are Claridge and Powell [6] and Povlau [7]. In both these works, the focus was on fatigue crack growth. Claridge and Powell used a form of the rainflow counting method to estimate the crack life of a forged alloy for aerospace engine application put under varying load profile. The authors found the predicted life to be within 50% of their experimentally obtained life. Povlau used the same software code to predict the strain hardening in the crack tips.

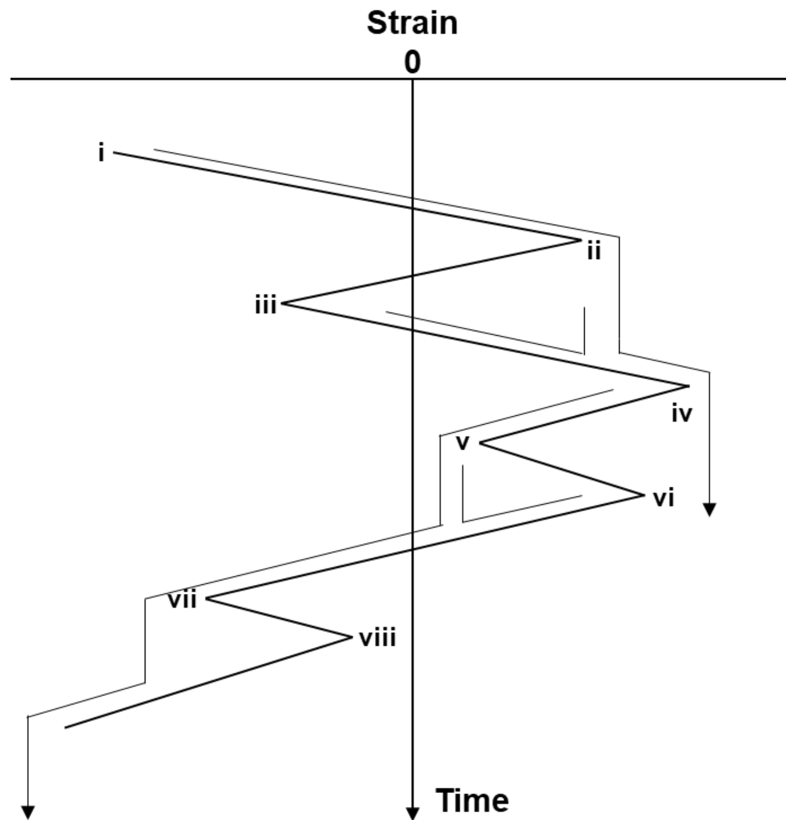

Figure 8. Rainflow counting of stress-strain cycles

Since then, thew algorithms has undergone significant evolution that improves it as well as makes it applicable to a wider range of applications. Probably the most popular form of this algorithm was presented by Downing and Socie created one of the most widely referenced and utilized rainflow cycle-counting algorithms in 1982 [8], which was then standardized as one of many cycle-counting algorithm [9]. The counting of a cycle using this algorithm employs the 3-point counting rule with equivalent data information and has been widely implemented for fatigue analysis studies in wind turbine components, among others.

Rychlik gave a mathematical definition for the rainflow counting method in terms of the toplevel-up cycle counting method and by showing that toplevel-up and rainflow counting are equivalent. [10]. This allowed for closed-form computations from the statistical properties of the load signal. Monte Carlo simulations or the narrow-band approximation and corrective factors were also commonly used for optimization [11].

While other counting methods are simpler, the rainflow counting method and its variants has the advantage of taking sequence effects into account, i.e. a cycle is influenced by the cycle preceding it. It makes these methods more conservative than other methods and more popular for stress-life and strain-life calculations. For example, in a comparison with rainflow counting, peak and level counting methods have been shown to overestimate life by 35% and 21% respectively [2].

2.2 Rainflow counting in life prediction of electronics

More recently, rainflow counting has been used in predicting lifetimes of electronic devices and assemblies, especially for real-time health management of electronics, which is also sometimes referred to as "reliability monitoring." In these applications, it is useful to identify an appropriate cycle counting method to generate regular spectrums of load profiles with varying frequencies and

amplitudes. This approach was first proposed by Pecht who showed with experimental validation that a rainflow counting based approach can provide sufficiently accurate lifetime predictions [12]. Pecht proposed a model that combines a physics of failure (PoF) approach with rainflow-aided damage accumulation to calculate the consumed and remaining life of electronic devices [13]. The proposed method inputs data as temperature or vibration and then calculates the cycles to failure based on empirical correlations, such as the Coffin-Manson or Basquin model [14, 15]. The Basquin model for elastic strain is given in equation (1).

$$\frac{\Delta\varepsilon_e}{2} = \frac{\sigma_f}{2E}(2N_f)^b \tag{1}$$

where $\Delta\varepsilon_e / 2$ is elastic deformation for a single half-cycle, N_f is the no. of cycles, σ_f is the fatigue strength coefficient and b is the Basquin constant. The Coffin-Manson model for plastic strain is given in equation (2).

$$\frac{\Delta\varepsilon_p}{2} = \varepsilon_{pf}(2N_f)^c \tag{2}$$

where $\Delta\varepsilon_{pf}$ is the fatigue ductivity coefficient, c is the fatigue ductivity exponent constant The cyclic damages are then added up according to Miner's rule and with the aid of rainflow counting.

As a means of enhanced characterization, Musallam et al. used a compact thermal model as an intermediary between the input and the output [16]. The compact thermal model was used to estimate the damage parameters, such as cycle characteristics and frequencies, and the damage parameters were then used to estimate life with the aid of rainflow counting. Knowledge of the life consumed for each different cycle then allows for the remaining life time to be estimated under operational conditions comprising of random loading. The authors used this approach to successfully model wire bond joints fatigue and crack growth in solder due to repeated temperature

cycling. Predictions of bond wire fatigue failure and crack length can be used to give information about the remaining life, thus making this technique a tool for prognostic health management of power electronic modules.

There has also been significant recent work in using rainflow counting for power electronics, especially as electrification of various industries make power electronics reliability becomes even more important due to their exposure to more demanding environments. Chen et al. obtained the online (real-time operational) junction temperature curve for IGBT modules by combining a rainflow counting method and a Foster network model with a lifetime prediction theory, for a three-level traction converter [17]. In addition, the feedback of thermal resistance changes was utilized to improve the lifetime consumption calculation accuracy. GopiReddy and Ozpineci [18] presented a modified version of the algorithm for IGBT life prediction in a static compensator (STATCOM). The authors demonstrated the algorithm's performance by studying its execution time and memory usage.

Counting algorithms are used widely as a way of identifying local minima and maxima pairs to determine equivalent load cycles. Usually, this counting method considers the entire time history of the load (the mission profile) as an input, and the equivalent cycles are then determined at the end of that time history. This approach works because most algorithms start the counting sequence at the highest maximum or lowest minimum value, something which can only be determined once a full data set is captured. Hence, for continuous time series data, an appropriate length of time history have to be chosen before the data is processed in blocks. This approach requires significant computational resources due to parallel processing of a lot of data. This becomes even more challenging when dealing with real time data from hybrid or electric vehicles, which consists of

large number of cycles that may be significantly smaller than the overall peaks (e.g. maxima and minima during a trip).

2.3 Summary and Conclusion

For loading profiles that are non-uniform and variable, cycle counting methods are a tool that can be used to analyze and quantify them. There are several types of cycle counting methods that can be used, but rainflow counting is suitable where sequence effects are important. That, or a simplified version, range counting, which recreates full cycles based on half-cycles, can be used for electronics reliability in conjunction with Miner's damage accumulation correlation. This would make them well suited for analysis of electric or hybrid vehicle loading profiles, which have varying load levels and large number of transient peaks. Next chapter will outline efforts to integrate a counting algorithm into a model to predict reliability and consumed life of automotive power electronic devices based on the vehicle's mission profile.

2.4 References

1. M. A. Miner, "Cumulative damage in fatigue," J. Appl. Mech. Trans. ASME, vol. 12, pp. A159–A164, 1945.

2. Stelzer, R., B. Carlton, and S. Mazzoni. "COMPARISON OF CYCLE COUNTING METHODS FOR POTENTIAL LIQUEFACTION AND STRUCTURAL FATIGUE ASSESSMENT."

3. M. Matsuishi and T. Endo, "Fatigue of metals subjected to varying stress," Japan Soc. Mech. Engineering, 1968.

4. S. Ariduru, Fatigue Life Calculation by Rainflow Cycle Counting Method 2004 [Online]. Available: http://wind.nrel.gov/designcodes/papers/FatLifeCalcByRFCycleCountingMeth_Ariduru.pdf

5. M. Meggiolaro and J. Pinho de Castro, "An improved multiaxial rainflow algorithm for non-proportional stress or strain histories," International Journal of Fatig ue, vol. 42, pp. 194–206, 2011

6. Claridge, S. R., and B. E. Powell. "Fatigue crack growth life predictions for single and dual amplitude loadings." WIT Transactions on The Built Environment 19 (1970).

7. Pavlou, D. G. "The influence of the crack tip plastic zone strain hardening on the metal high cycle fatigue behavior." WIT Transactions on The Built Environment 35 (1970).

8. Downing, Stephen D., and D. F. Socie. "Simple rainflow counting algorithms." *International journal of fatigue* 4.1 (1982): 31-40.

9. ASTM, ASTM E. "1049–Standard practices for cycle counting in fatigue analysis." *West Conshohocken (PA)* (2003).

10. Rychlik, Igor. "A new definition of the rainflow cycle counting method." *International journal of fatigue* 9.2 (1987): 119-121.

11. Metropolis, Nicholas. "The beginning of the Monte Carlo method." *Los Alamos Science* 15.584 (1987): 125-130.

12. Pecht, Michael. "Prognostics and health management of electronics." *Encyclopedia of structural health monitoring* (2009).

13. Ramakrishnan, Arun, and Michael G. Pecht. "A life consumption monitoring methodology for electronic systems." *IEEE Transactions on Components and Packaging technologies* 26.3 (2003): 625-634.

14. Coffin Jr, L. F. "Discussion: "The Failure of Structural Metals Subjected to Strain-Cycling Conditions"(Swindeman, RW, and Douglas, DA, 1959, ASME J. Basic Eng., 81, pp. 203–208)." *Journal of Basic Engineering* 81.2 (1959): 208-209.

15. Concer, D., N. Woellner, and P. V. P. Marcondes. "Approach to the prediction of thermal fatigue of aluminium high pressure die casting (AISI H13) using the Basquin equation and finite elements." *Journal of Achievements in Materials and Manufacturing Engineering* 55.2 (2012): 439-445.

16. Musallam, Mahera, et al. "In-service life consumption estimation in power modules." 2008 13th International Power Electronics and Motion Control Conference. IEEE, 2008.

17. Chen, Zhiwen, et al. "Converter lifetime modeling based on online rainflow counting algorithm." 2019 IEEE 28th International Symposium on Industrial Electronics (ISIE). IEEE, 2019.

18. GopiReddy, Lakshmi, Leon M. Tolbert, and Burak Ozpineci. "Lifetime prediction of IGBT in a STATCOM using modified-graphical rainflow counting algorithm." *IECON 2012-38th Annual Conference on IEEE Industrial Electronics Society*. IEEE, 2012.

Chapter 3. Development of Mission Profile Dependent High-Fidelity Thermal Behavior Modeling Tool for Electric Drivetrains

A mission profile is the representation of all relevant loading conditions that a vehicle (or component) will be exposed to during its operational life [1]. In reliability analysis, therefore, mission profiles act as the starting point and usually encompass the standard driving cycle and the environment conditions such as ambient temperature [2]. While mission profiles present the electric or hybrid electric vehicles with a defined application in terms of reliability assessment, but the mission profile of the vehicle may differ from the mission profiles of its critical components. For a hybrid or electric vehicle, the vehicle mission profile is usually its drive cycle, charting its speed over a certain time. For its drivetrain components, the mission profile will be the power it must expend in order to result in a certain acceleration for the car overall. The component-level mission profiles can have a significant impact on the semiconductor devices in the powertrain due to the thermal stresses that develop as a result of heat dissipation. The mission profiles are not independent, as applications-specific requirements are handed down from the larger system to the smaller sub systems and components. External or environmental stresses, such as air resistance due to wind or added tractive power necessary to overcome a steep road, will mean that for the same vehicle drive schedule, the powertrain will have to transmit more power to the wheels, resulting in higher dissipation in the power electronics devices. The various factors that affect the mission profiles at various system/component levels are illustrated in Fig. 9. The effect is passed rightwards as the need of the vehicle has to be met by the powertrain, and the requirements of the powertrain to come from the power electronic devices.

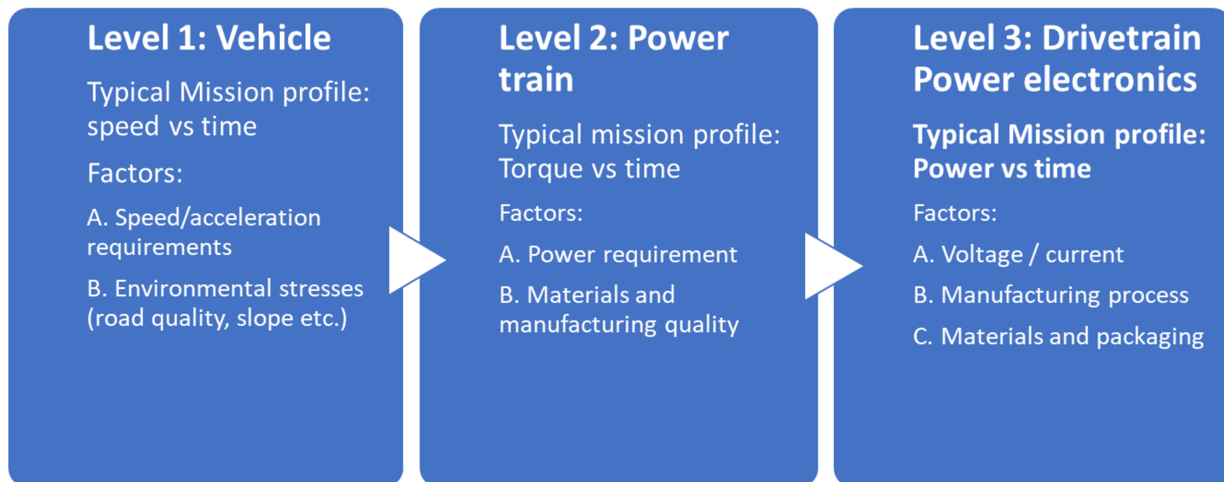

Figure 9. Various hierarchical levels in a typical electric vehicle propulsion system, their associated mission profiles and factors that affect them

In order to understand and assess the reliability of power electronics (level 3 in Fig. 9) it is therefore imperative to start from the drive cycle. The drive cycle, or drive schedule, will have a direct relationship on the powertrain operational mission profile, which will then affect the currents and voltages in the semiconductor dies in the power electronics. The typical drive cycle looks like the ones shown in Fig. 10. It is an Urban Dynamometer Drive Schedule (UDDS) and the Highway Fuel Economy Test (HWFET) cycle are standard drive schedules that the Environmental Protection Agency (EPA) uses for fuel efficiency estimation of vehicles [2]. It is designed to mimic city driving conditions, with frequent stop-and-go situations. The UDDS is the type of drive schedule that is particularly harsh on critical components because of the high frequency of the resulting power and thermal variations. The HWFET, which represents highway driving conditions, is more uniform has fewer stops.

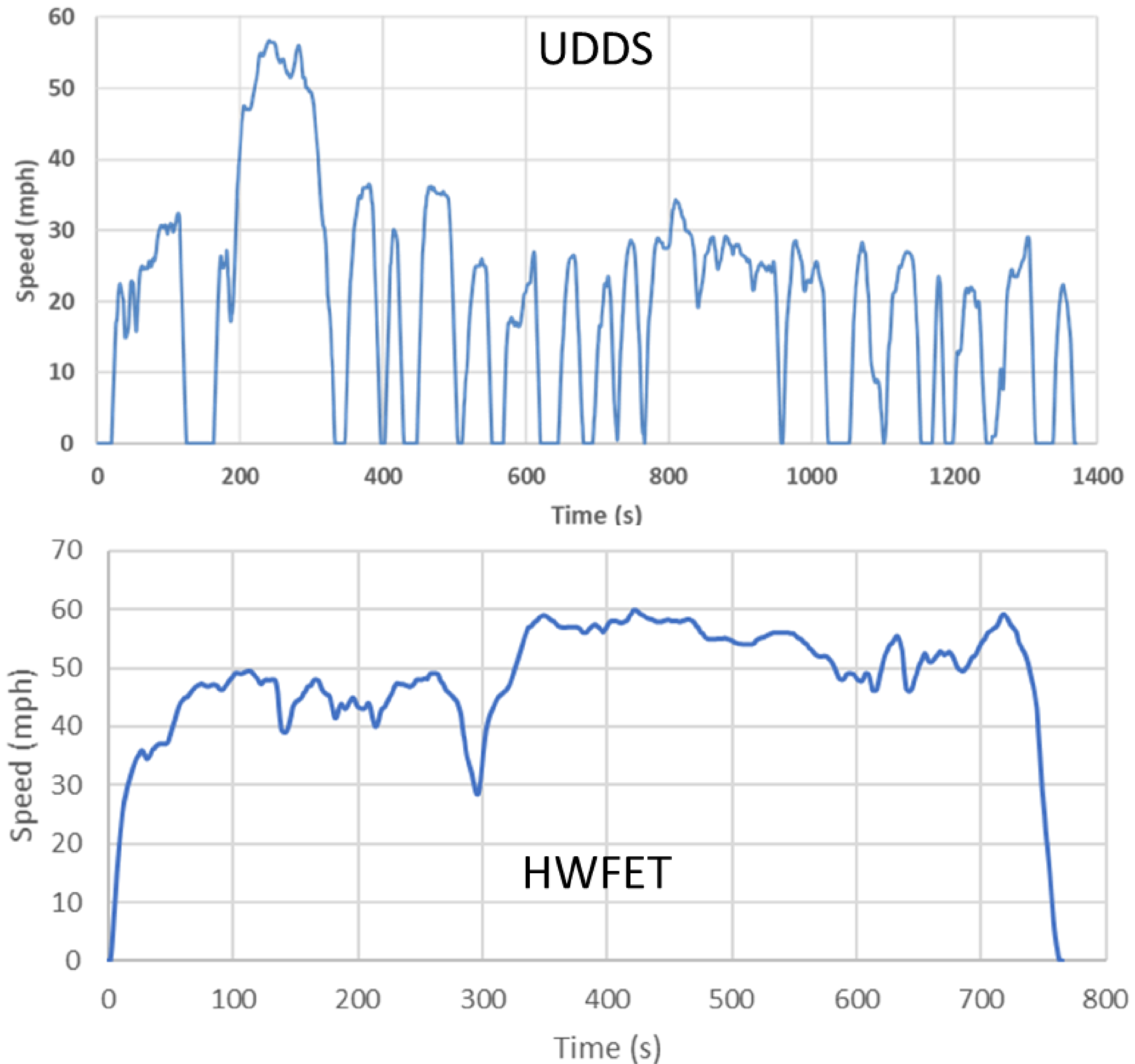

Figure 10. Urban Dynamometer Drive Schedule (UDDS) and Highway Fuel Economy Test (HWFET) drive schedule from the Environmental Protection Agency

In order to translate these drive schedules into reliability estimates, they must be used to derive a temperature profile that will be applicable at the electronic device level. There are two different levels of detail that this analysis has goes into: one that looks at the power devices as a single entity (first pass) and then looks at them in greater detail (second pass).

3.1 First Pass Analysis

Standard EPA driving cycles for different driving conditions were evaluated using reasonable approximation of the forces acting on the vehicle to calculate the total tractive force the vehicle would require at a given time in its travel. The motor power output is calculated based on the tractive force, and the losses are assumed to be dissipated as heat through the inverter. The force, torque and power are calculated assuming the parameter values given in Table 3 (refer to Appendix A1 for example calculation). They are based on the 2013 model of a popular, commercially available hybrid passenger vehicle [##].

In order to make the drive schedules useful, they must be utilized to extract the temperature profiles at the power electronics level. As noted earlier, inverter carries out the function of converting direct current (DC) to alternating current (AC). The main semiconductor components in the inverter are the switching dies and the diodes. They are packaged as power modules and are often connected using a busbar to capacitors and gate drivers. In order to ensure operation within reasonable temperature range, the assembly is coupled to a heat sink.

Table 3. Vehicle-specific parameters used to calculate force and power based on drive schedule

Parameter	Value	Units
Coefficient of rolling friction	0.012	
Vehicle mass	1300	Kg
Air density	1.3	Kg/m^3
Frontal area	2.65	m^2
Tire radius	0.2	m
Gravity, g	9.81	m/s^2
Aerodynamic drag coefficient	0.6	
Grade or inclination angle	0	Degrees
Friction factor that account for frictional losses between bearings, axles, (10-15%),Rf	1.1	
Gear ratio	20	

In the first pass analysis, the entire power module-capacitor-busbar-gate driver assembly is simplified into a single discrete body with uniform volumetric heat generation connected to a simple flat plate heat sink. The heat is assumed to be dissipated through a flat plate heat sink made of aluminum (Fig. 11). The heat sink base is a rectangle of dimensions 15 cm by 10 cm, with 10 fins, each 2 mm thick and 6 cm high, giving a heat transfer area of 0.196 m^2. The heat sink specifications are listed in Table 4, and are taken from an available, commercial heat sink widely used for such purpose. The fluid flow is considered to be along the channels. The resistance to heat flow in the heat conduction path between the module and the heat sink is assumed to be very small, so that the heat sink and the inverter are considered to be at the same temperature. The other major assumption is that the heat sink-inverter assembly is a lumped mass. This is based on the fact that the Biot number for the heat sink is significantly less than 0.1 for all values of convective heat transfer coefficient considered in this study, which would lower the Biot number for the system. The system should therefore approximately model a lumped mass but a second pass analysis is described later that will take into account specific geometric and material parameters of the system.

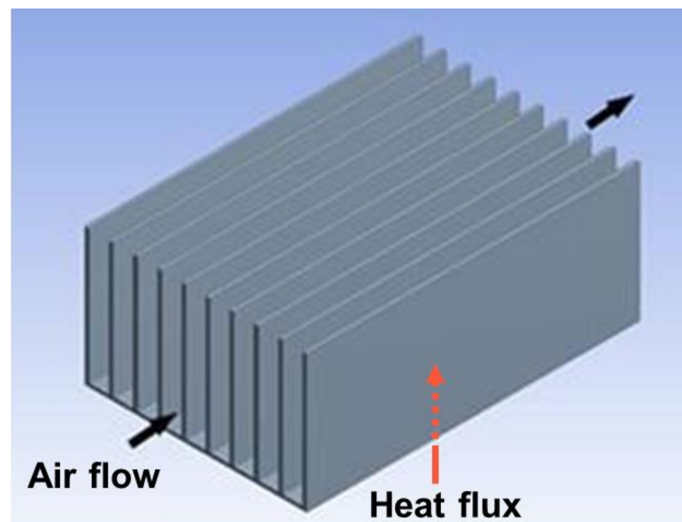

Figure 11. Heat sink with direction of fluid flow indicated

Table 4. Heat sink specifications		
Length, L	0.15	m
Width, W	0.1	m
Fins	10	
Height, H	0.06	m
thickness, t	0.002	m
Conductivity	237	W/mK
Fin Area, A_{fin}	0.183	m^2
Base Area	0.0129	m^2
Surface Area, A_s	0.1959	m^2
Volume, V	0.00018	m^3
Density, ρ	2700	Kg/m^3
Specific Heat	900	J/kg K

Figure 11 indicates the fluid flow and heat flux direction. The coefficient of heat transfer is assumed to be constant over the entire exposed area of the heat sink. The process of translating the drive schedule to a temperature profile is done in a series of steps, which are outlined below:

Step 1. Calculation of instantaneous accelerations based on numerical differentiation at each time step

Step 2. Use the acceleration to compute the required force and torque based on parameters listed in Table 3.

Step 3. Calculate the required motor output.

Step 4. Based on the motor output calculated in step 4 and assuming efficiency to be 97%, estimate the heat dissipated (Q) in the power electronics semiconductors.

Step 5. Temperature is calculated at each time step using equation (1) below.

$$\frac{T-T\infty}{T_i-T\infty} = exp(-at) + \frac{b/a}{T_i-T\infty}[1 - exp(-at)] \quad \textbf{(1)}$$

where $a = \frac{h.A}{\rho.V.Cp}$ is the time constant and $b = \frac{\dot{E}_g}{pVc}$ is the power dissipation term. The process of translating drive schedule to temperature profile in this way is illustrated in Fig. 12. So, the drive schedule is first used to derive a power schedule, which acts as an input in the process of finding the temperature profile. The $\dot{E}_g$ in equation (i) is the power or Q from the power dissipation curve.

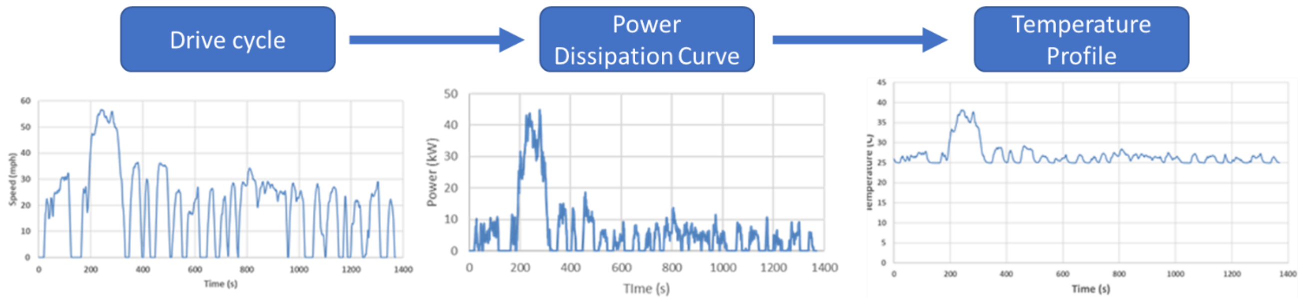

Figure 12. Deriving temperature profile from drive schedule for UDDS

The advantage of this approach is simplicity and inexpensiveness in terms of computational power and time to change the boundary conditions and simulate. Figure 13, for example, presents the results of changing the coolant temperatures on the temperature profile for a constant coefficient of convection. As this model does not take into account the thermal capacitances of the system components, it is not able to predict the temperature rise times. This is one significant source of inaccuracies in this model. Figure 14 shows the temperature profile resulting from another EPA drive schedule, the Highway Fuel Efficiency Test cycle, and the effect of road grading. A positive road grading (sloped upwards) results in a temperature profile that is consistently higher and a

negative slope shows the opposite. This is an example of external conditions affecting the mission profiles at the power electronic device level.

The main purpose of developing this first pass is to pave the way for a more refined model. The major shortcomings of the first pass is the lack of details about the thermal capacities. This results in temperature predictions dominated by ambient temperatures. This can be improved by taking into account the thermal capacities of the bodies, instead of the lumped mass assumption in pass 1. The second pass will build on this by taking the inverter to be composed of the individual components rather than a single-body system.

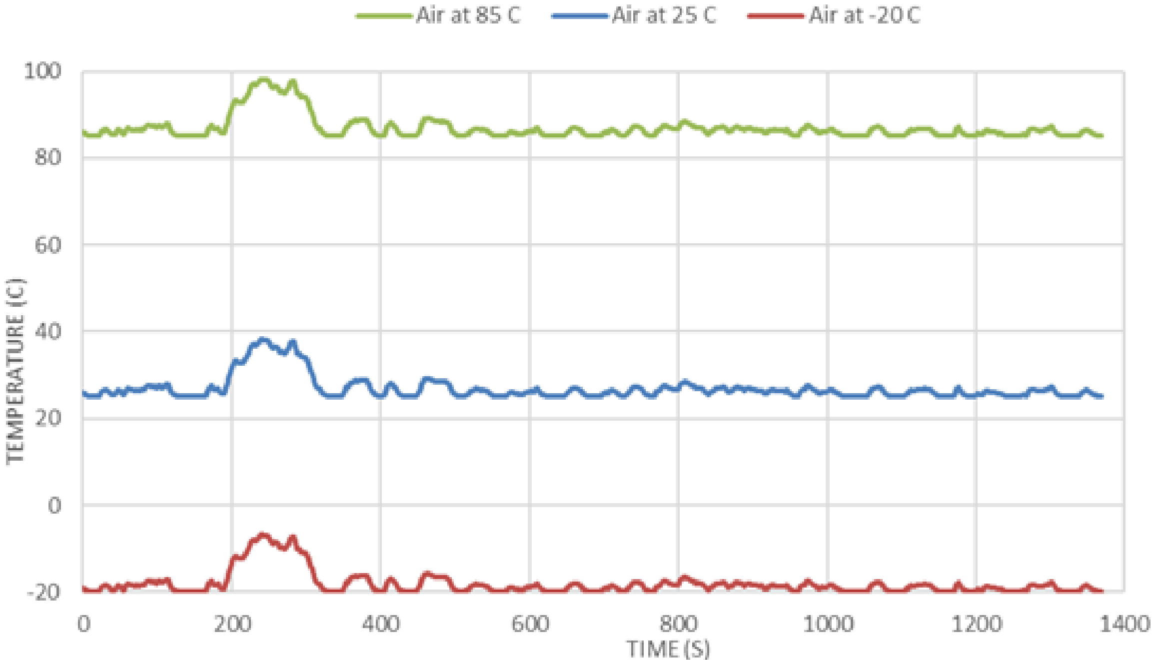

Figure 13. Predicted Temperature profile variation with air temperature, assuming air is the coolant

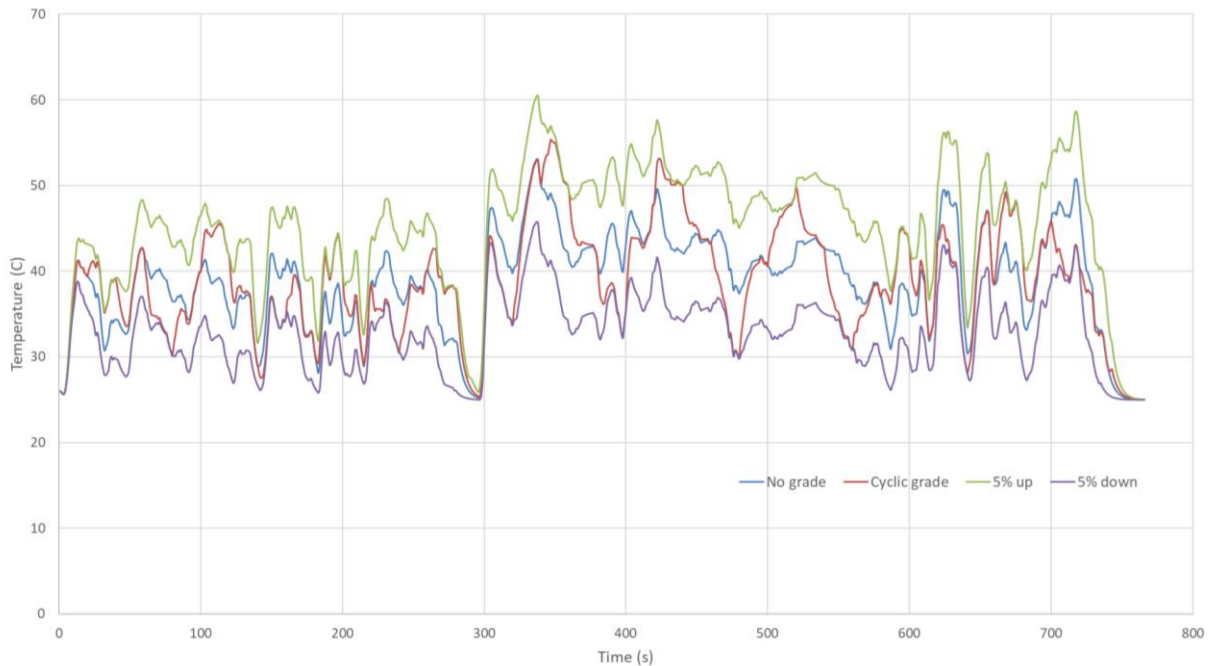

Figure 14. Predicted Temperature profile variation with air temperature, assuming air is the coolant

3.2 Second Pass Analysis: Lumped Capacitance Thermal Circuit Model

While the analyses discussed in the previous section is useful, they are very limited in terms of accurate thermal and reliability predictions due to their simplifications in their thermal properties. A lumped capacitance (LC) circuit can provide a more representative model and can provide improved understanding of the system and component behavior from a thermal viewpoint. An actual inverter is used to create the lumped capacitance model.

The inverter modeled in the following analysis is based on a 250 kW three-phase all-SiC three level T-type prototype that the University of Arkansas is developing for traction applications (Fig. 15). The design consists of six half-bridge modules connected to six DC-link capacitors through a busbar. The system is cooled by flowing water-ethylene glycol mixture through a liquid-cooled cold plate. The thermal circuit diagram of the inverter is illustrated in Fig. 16.

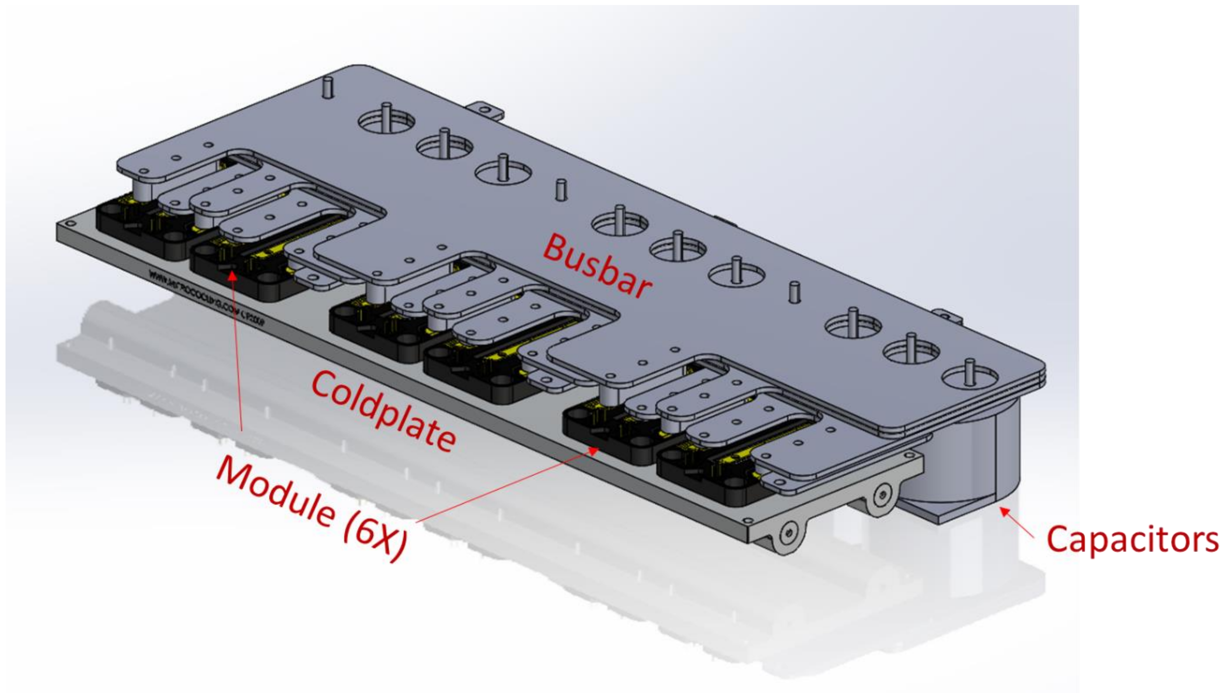

Figure 15. CAD drawing of 250 kW three-phase all-SiC three level T-type

Table 5. Values of parameters shown in Figure 14

Parameter	R (K/W)	Parameter	C (J/K)
R_conv	2.8E(-3)	C1	4385.8
R1	0.135	C2	126.3
R2	0.135	C3	674.7
R3	0.31	C4	51.4
R4	0.1	C5	1344
R_amb1	0.96		
R_amb2	0.210		

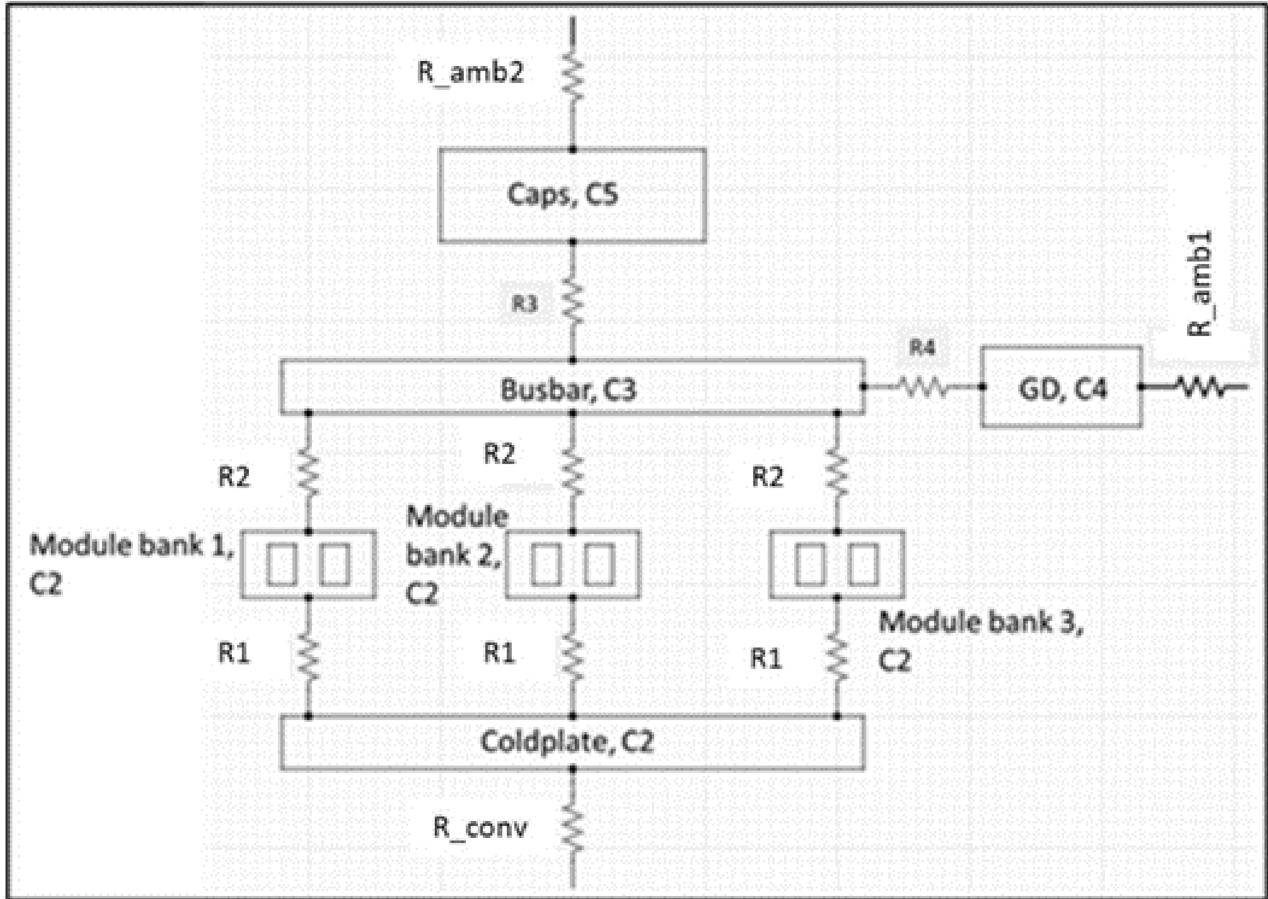

Figure 16. Equivalent lumped capacitance (LC) thermal circuit of 250 kW three-phase all-SiC three-level inverter system

The values of the parameters in Fig. 14 were calculated based on material properties and actual dimensional measurements. In some cases, manufacturers' data sheet were consulted to estimate the properties based on internal geometries. The values are listed in Table 5. The code, including the equations used to compute temperature, can be found in Appendix A2.

3.3 Testing and Validation of Model

In order to validate the parameter values and the model itself, the inverter was powered up to 75 kW and coolant was flowed through the cold plate at 12.6 C (Fig. 17). The cold plate surface temperature and capacitor temperature were measured using a thermocouple connected to a data acquisition system. An infrared imaging camera was pointed at the gate drivers to estimate their

temperature. The data was used to summarize their heating profile as the inverter is powered up from an off state. The actual heating curve is compared to the predicted heating curve based on the model. The charts are shown in Fig. 18. The capacitor temperature has two dips. This was most likely an issue with the thermocouple. The overall trend, however, is consistent and shows an increase in capacitor temperature with time.

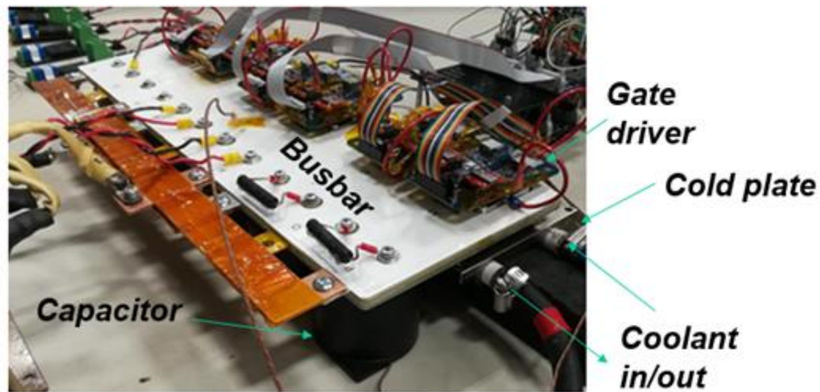

Figure 17. Experimental setup

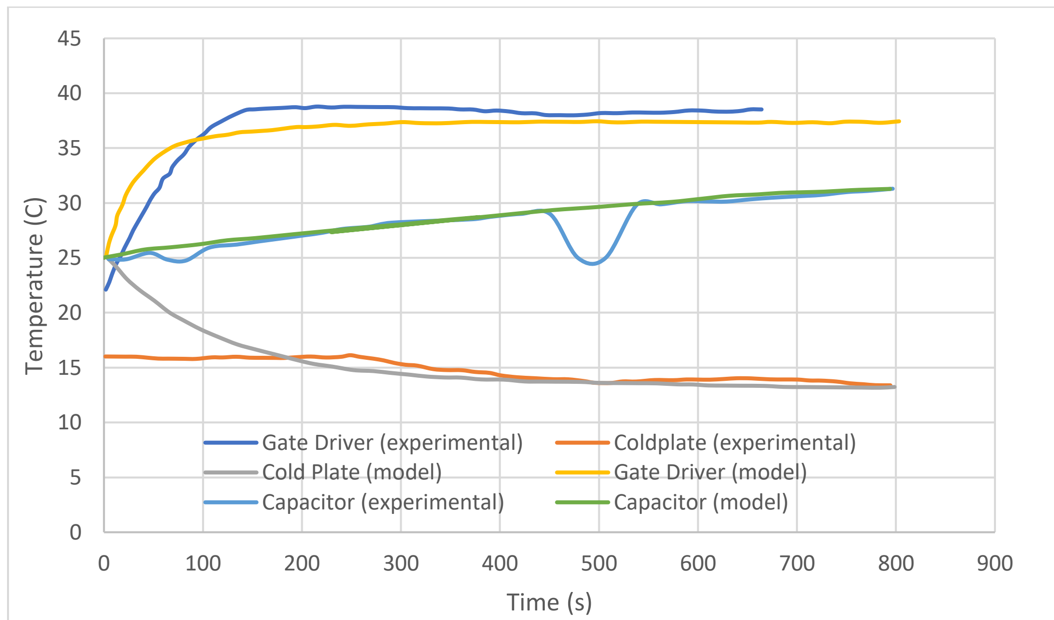

Figure 18. Comparison of lumped model prediction with test data

Table 6. Comparison of steady state temperature and rise time for cold plate and gate drivers from LC model with experimentally measured temperatures.

	Experimental	Model	% difference
	Steady state temperature (^{0}C)		
Gate driver	39.0	37.8	0.06%
Cold plate	13.9	13.8	0.04%
	Rise time (s) (99% of steady state)		
Gate driver	180	220	22%
Cold plate	380	270	28%

The results are shown and compared in Table 6.

There are several possible reasons for this discrepancy, among which are the approximations regarding the internal volume of the cold plate and the surface area subject to convection by the coolant. Both affect the thermal resistance and capacitance values used in the model and therefore would affect the numerically calculated temperature. For the gate drivers, the temperature plotted in Fig. 18 are the hot spot temperatures, which is the probable cause behind the difference with the model predictions. However, there is still reasonable agreement, especially for temperature values (Table 6) and therefore the general fidelity of the model is confirmed.

The main factors affecting the cold plate temperature in the experiment were

a. The heat dissipated in the dies

b. The coolant inlet temperature

c. The effective coefficient of heat transfer (h)

d. Exchange of heat with surroundings (for cold plate)

Ideally, part (d) should be negligible. To be certain, an energy analysis of the system was carried out based on the coolant inlet/outlet temperature. Heat flow (heat carried away by the coolant) was measured over a repetitive interval using numerical integration, and just assuming that to be all the heat dissipated resulted in a calculated efficiency of 98.9%, which is very close to the predicted efficiency of 99%. The heat lost to (or gained from) the surroundings, in this case, is very small. The difference is likely due to convection from the gate drivers and capacitors to the surroundings.

3.4 Summary

This chapter outlines the analyses accompanying the development of a thermal model that takes the mission profile as input, then derives from it the mission profiles at the component level. The aim is to create an accurate temperature profile of the drivetrain power electronics, as they would be under the most intense thermal environment.

The first pass is an oversimplified version that assumes the inverter to a single body that is dissipating heat to the surroundings. Although inherently limited in scope, it allows for visualizing changes in the thermal profiles based on changes in boundary conditions. Its main limitations arise from the fact that it simplifies the inverter-heat sing assembly as a single, discrete body that is assumed as a lumped mass. The second pass builds on this in multiple ways: instead of a single lumped mass, the system is broken down into a collection of lumped masses that each represent a component, and the connection between each component are modeled as thermal resistances. In order to create a realistic model, the dimension and material property values are obtained from an actual powertrain inverter. The model was then validated against test data, and reasonable accuracy was found. The model will be discussed in the next chapter in terms of reliability estimation.

3.5 References

1. https://semiengineering.com/mission-profiles-in-the-automotive-development-process/

2. I. Vernica, H. Wang and F. Blaabjerg, "A Mission-Profile-Based Tool for the Reliability Evaluation of Power Semiconductor Devices in Hybrid Electric Vehicles," *2020 32nd International Symposium on Power Semiconductor Devices and ICs (ISPSD)*, 2020, pp. 380-383, doi: 10.1109/ISPSD46842.2020.9170201.

3. Nirmaier, Thomas, et al. "Mission profile aware robustness assessment of automotive power devices." *2014 Design, Automation & Test in Europe Conference & Exhibition (DATE)*. IEEE, 2014.

4. https://www.epa.gov/vehicle-and-fuel-emissions-testing/dynamometer-drive-schedules

Chapter 4. Rainflow Counting and Damage Accumulation Due to Thermal Transients

The previous chapter introduced drive schedules as mission profiles for hybrid and electric vehicles, and discussed the different mission profiles that the components may be subject to. A way of translating the drive schedule to a temperature profile for the component was also presented, particularly with a focus on the power electronics. The temperature profiles in the power electronics will be dominant factors in deciding their longevity and reliability. The temperature profile provides key information about stressors and damage-inducers such as the maximum and minimum temperatures (the difference being the temperature swing, or ΔT), number and frequency of temperature swings, the mean and medium temperatures, and can be used to estimate the resultant thermomechanical stresses due to thermal expansion mismatch.

In order to predict the reliability based on drive schedules, the drive schedules will first have to be used to extract the temperature profiles, which can be done based on the lumped capacitance model presented in the previous chapter. In this study, three different drive schedules will be studied in order to investigate the sensitivity on reliability. They are chosen so as to be representative of different mission profiles or driving environments that electric drivetrains may be subject to. The first is the Urban Dynamometer Drive Schedule (UDDS) discussed in the previous chapter (Fig. 19 (a)). It is an Environmental Protection Agency (EPA) drive schedule that the agency uses to estimate fuel efficiency in city driving conditions [1]. The second is the Highway Fuel Efficiency Test (HWFET) drive schedule, also from the EPA, that is used to mimic highway driving (Fig. 19 (b)). The third is an EPA off-road drive schedule for an agricultural tractor (Fig. 19 (c)). With drivetrain electrification ongoing across industries, agricultural and heavy machineries are no exception. So this is chosen to be representative of such commercial or agricultural vehicles. In order to facilitate a reasonable comparison, they have been expressed as a percentage of their

maximum speeds rather than any nominal speed. This will make a comparison between the three drive schedules easier when the same inverter system is used.

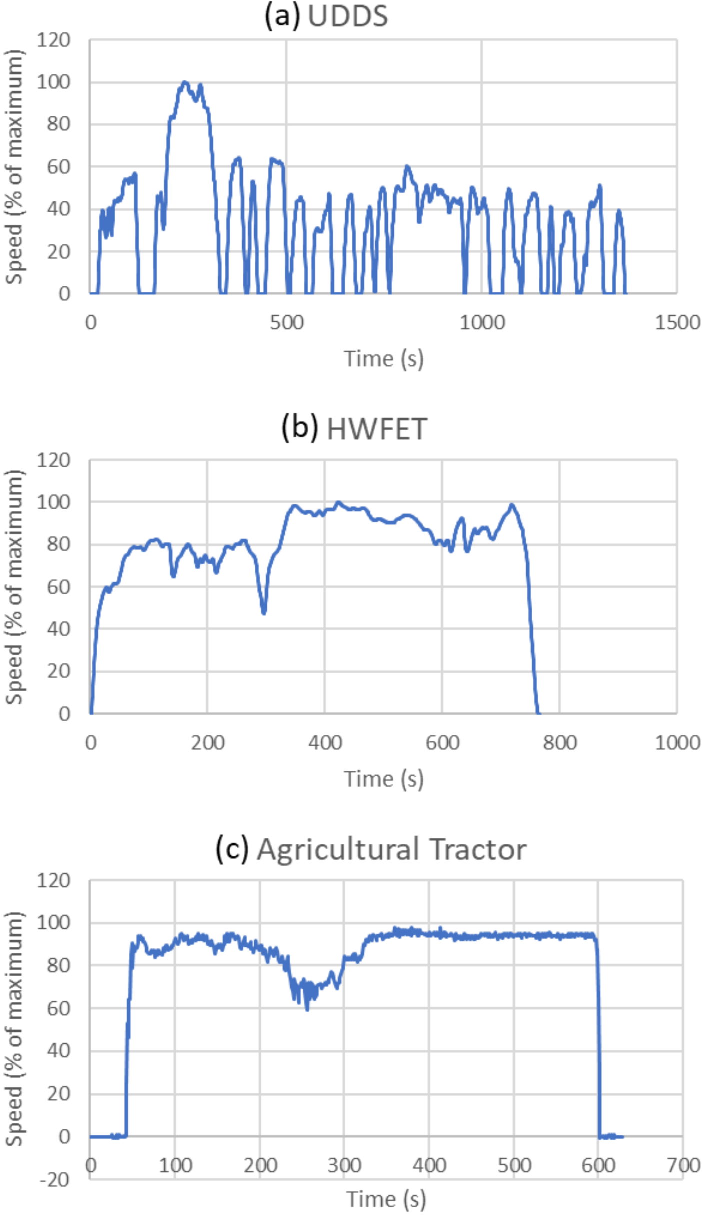

Figure 19. Drive schedules considered in this study, speed expressed as a ratio for ease of comparison

In order to effectively quantify their parameters as representative of actual operational conditions, the drive schedules are repeated and adjusted to make them continuous. Apart from the startup

portion, the rest of the drive schedule, corresponding to stable operation, was repeated. Fig. 20 shows the agricultural tractor profile extended to be representative of long duration operation.

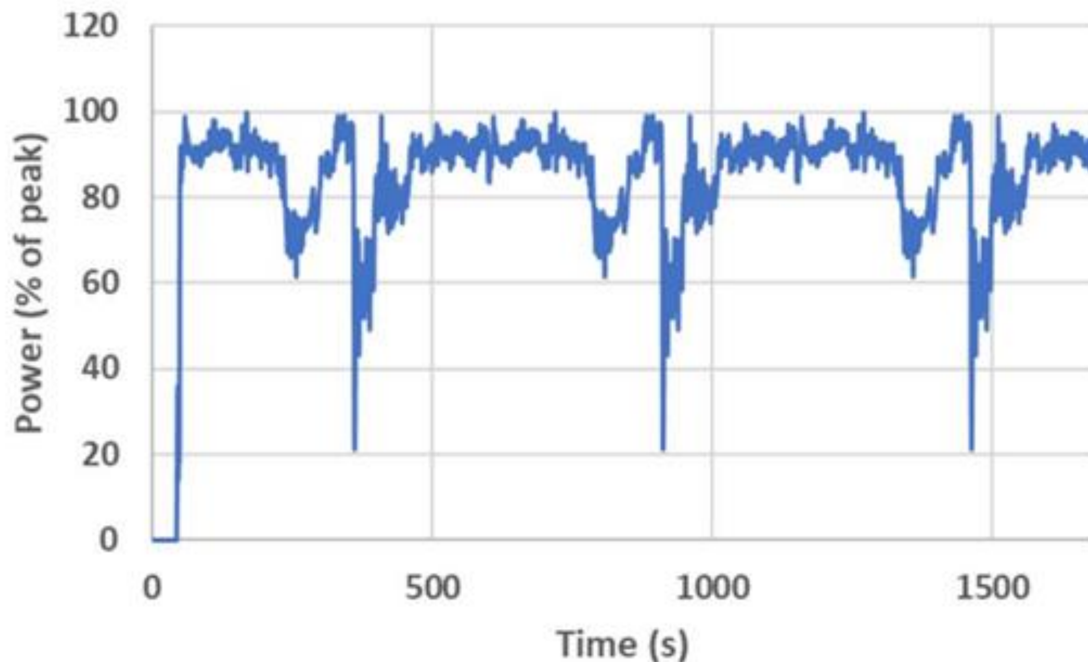

Figure 20. Continuous version of agricultural tractor drive schedule shown in Fig. 19 (c)

4.1 Temperature profile estimation

In order to predict the thermal profile, the model developed and validated in the previous section is used. The drive schedule is used to create the power schedule (power vs time). The power is scaled for a maximum of 200 kW, or 80% of the rated power, to be consistent with the inverter that was used for validation purposes (Chapter 3). The coolant temperature is taken to be 105 C. It is so chosen because a coolant consisting of 50:50 mixture of water and antifreeze (ethylene glycol) vaporizes at 106 C, so 105 C is the highest temperature at which it can maintain its cooling functionality. The ambient temperature is taken to be 70 C. This is approximately the expected temperature within the inverter enclosure based on simulations.

The drive schedules were fed into the model outlined in Chapter 3 to extract the temperature profiles of the various components. The power dissipation mirroring the drive schedule was set as a boundary condition in the power modules, and initial temperature was set at 25 C. The components each had associated differential equations which were solved simultaneously. The geometric and materials are used to extract the resistances and capacitances required to solve the model. The temperature profiles of the different components obtained using the lumped capacitance model is given in figure 21 (a-c).

Simply from visual inspection, some features are clear from Fig. 21:

i. The power module temperature closely follows the mission profile. This is to be expected as all the power necessary goes through the power modules and assuming constant efficiency, the heat dissipated will be roughly proportional to the power.

ii. The gate drive feels some of the transient effect, but not to the same extent.

iii. The capacitors achieve steady-state after a long interval. This is due to the thermal mass of the capacitors due to the materials they are made from.

iv. The cold plate (heat exchanger, or ‘HX’ in Fig. 21) comes to the same temperature as the coolant fairly quickly. This is due to the high surface area of convection provided to the coolant fluid.

Now that the temperature profiles have been extracted and a visual assessment was carried out, the next step will be to investigate their characteristics more thoroughly in order to understand the value of the failure stressors and what effect they may have on the reliability of the components.

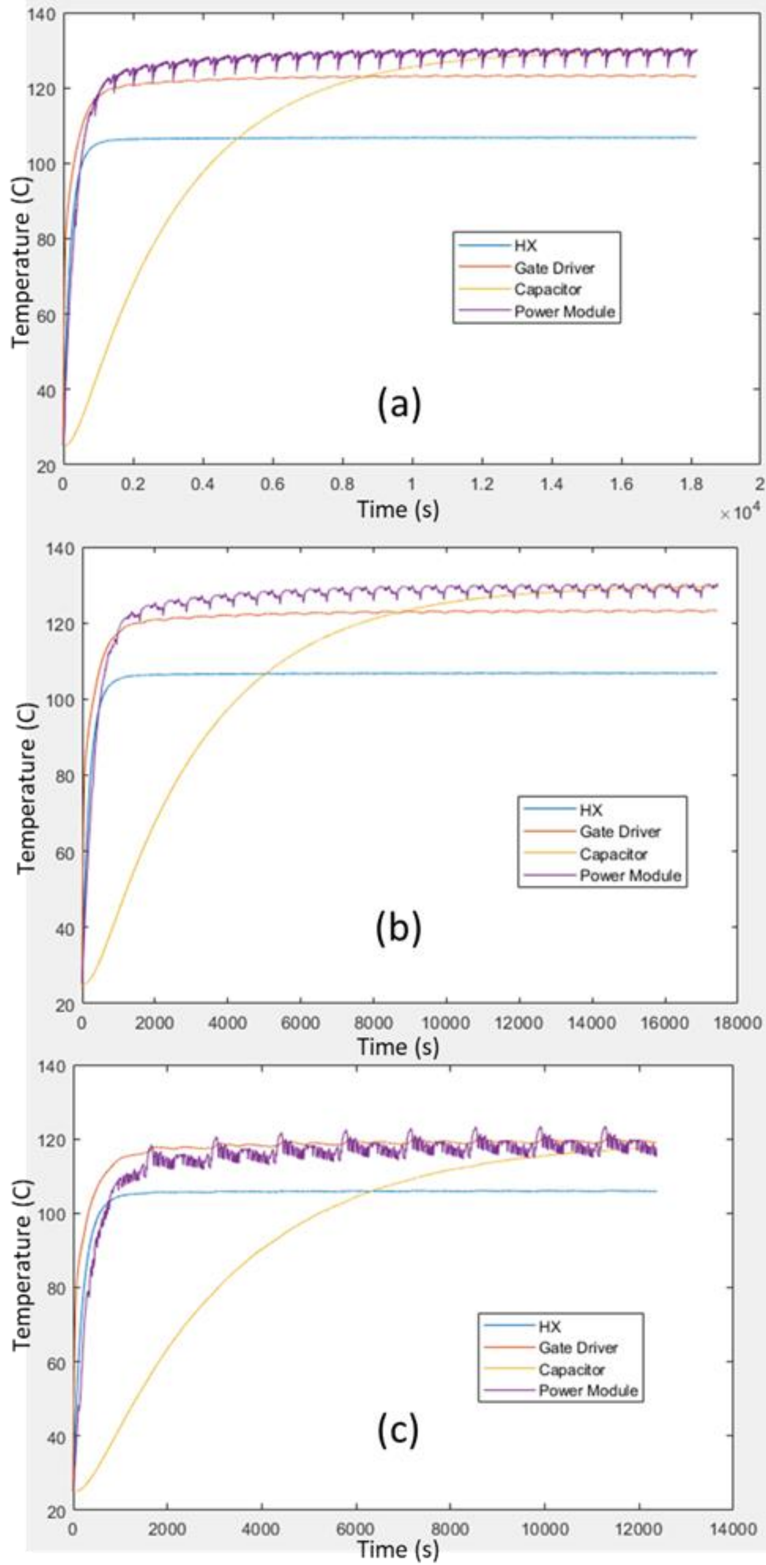

Figure 21. Temperature profiles for components obtained from mission profiles (a) UDDS, (b) HWFET and (c) Tractor

4.2 Drive schedules applied to LC model: mean temperatures, temperature swings, and effective frequencies

In order to extract the damage parameters from the thermal profiles, it is first necessary to separate the charts into two parts: the startup and the continuous operation part. The damage parameters are the failure drivers in power electronics that were discussed in Chapter 3, and include the temperature swing, mean and maximum temperatures, and effective frequency. They play key roles in deciding the cycles to failure, according to equations (1) and (3). The startup will have a large temperature delta but will only happen occasionally. The temperature deltas happening during continuous steady-state operation are smaller in magnitude, but take place more frequently and for longer duration. The two parts are divided approximately as shown below in Fig. 22 for HWFET drive schedule. The delineation is made based on the peak-to-peak variation. The duration when the peaks varied across repetitive cycles by more than 2% of the mean temperature was considered the startup region. The aim is to separate the startup/shutdown effect from regular operation. The two conditions will instead be looked at separately at first, and their combined effects will be discussed later.

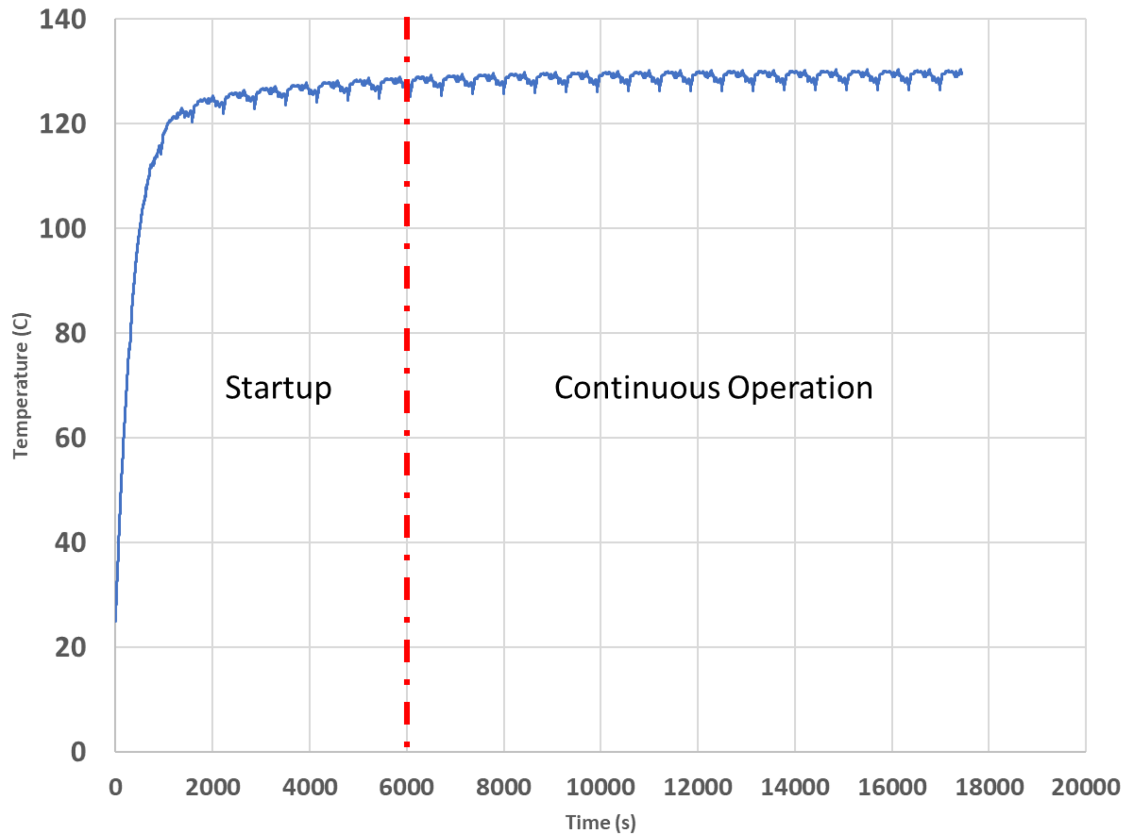

Figure 22. Temperature profile divided into startup and continuous segments

4.3 Reliability models and drive schedules compared

The next step is predicting the reliability and investigating correlations for any implications. This work will primarily look at interconnect reliability as they often limit the device reliability in electronic devices. Before we proceed further, it is important to note that in power systems, capacitors can often be the reliability limiter. The capacitor temperature predicted from the model, as shown in Fig. 21, exceeded the rated temperature of most conventional capacitors for DC-link applications. In this study, however, the inverter, and therefore the interconnects, are under focus.

The two most common types of interconnects used are solder bonds where the solder balls are arranged in a ball-grid array (BGA) shape, and bond wires [2]. A widely accepted correlation that

relates solder interconnect lifetime to the prevailing conditions is the Norris-Landzberg (modified Coffin-Manson) equation [3]. The relation is expressed as follows.

$$AF = \frac{N_O}{N_t} = \left(\frac{f_t}{f_O}\right)^a \left(\frac{\Delta T_t}{\Delta T_O}\right)^b \exp\left[\frac{E_a}{R}\left(\frac{1}{T_{max,O}} - \frac{1}{T_{max,t}}\right)\right] \quad (1)$$

Here, *AF* stands for acceleration factor, *N* stands for cycles to failure, E_a is the activation energy and *a* and *b* are exponents of frequency and temperature swing, respectively. The subscripts *t* and *O* correspond to test and operational conditions.

For SAC305, which is the most widely used lead-free solder used for bonding, *a* and *b* are 0.136 and 2.65 respectively, and E_a/R is equal to 2185 [4].

Another way of writing this equation is as follows [5].

$$lnN = \alpha_0 + \alpha_1 \ln(\Delta T) + \alpha_2 \ln(f) + \alpha_3\left(\frac{1}{T_{max}}\right) \quad (2)$$

This form of the equation will be used in the reliability assessment in this work.

The cycles to failure of a wire bonded device is given by Held's Arrhenius Coffin-Manson model [6].

$$N_f = A\, \Delta T^{\alpha} \exp\left(\frac{Q}{RT_m}\right) \quad (3)$$

Here, N_f is the number of cycles to failure, ΔT is the temperature swing and T_m is the medium temperature. The parameters consistent for aluminum bond wires are given in Table 7.

Table 7. Parameter values for aluminum bond wires

Parameter	Value

A	5.1E+09
α	-5
Q	29900
R	8.314

The damage due to each cycle is then summed to provide the cumulative damage according to Miner's rule [7]. The following notation can be introduced:

W = Relative total damage

w_i = amount of damage during single load mini cycle

n = No. of mini cycles

$$W = \sum_1^n w_i \tag{4}$$

If the damage accumulated in a single cycle is defined as a reciprocal of the acceleration factor when the cycle thermal characteristics are compared to those outlined in the JESD22 qualification,

$$W = \sum_1^n \frac{1}{AF_i} \tag{5}$$

Here AF_i is the acceleration factor for the i'th mini cycle.

4.3.1 Thermal Characteristics during Startup

A MATLAB code is used to ease the process of extracting damage-inducing parameters from the temperature profile. The code can be seen in Appendix A2**.**

The startup phase is much simpler to analyze as the key parameter here are the maximum temperature and the temperature delta (calculated by subtracting the minimum temperature from the maximum temperature). The values for the three drive schedules are shown in Table 8.

Table 8. Startup conditions compared for different mission profiles

Mission Profile	Minimum Temperature (C)	Maximum Temperature (C)	ΔT (C)	Mean Temperature (C)
UDDS	25	123.55	98.55	74.27
HWFET	25	130.40	105.40	77.70
Agricultural Tractor	25	130.80	105.80	77.90

The table above shows that UDDS has slightly smaller maximum temperature and ΔT than HWFET and the tractor, but as UDDS simulates urban, stop-and-go traffic, it may have more temperature variations during continuous operation.

4.3.2 Thermal Characteristics During Continuous Operation

The same program is used to derive the stress parameters from the continuous operation portion of the temperature profiles. This is done in order to facilitate quantification of thermal and reliability characteristics unaffected by startup and shutdown.

The parameters extracted are summarized in Table 9. The minimum and maximum temperatures, as well as the ΔT, are important, and are listed in Table 9 as well. However, medium temperatures (halfway point between maximum and minimum temperatures) and the effective frequencies are also listed, as they will play important roles in calculating reliability lifetimes according to Norris-Landzberg model.

Table 9. Key metrics from compared for different mission profiles for continuous operation

	UDDS	**HWFET**	**Agricultural Tractor**
Minimum Temperature (C)	113.8	126.3	123.8
Maximum Temperature (C)	123.6	130.4	130.8
ΔT (C)	9.71	4.13	6.97
Mean Temperature (C)	118.1	129.22	129.2
Medium Temperature (C)	118.7	128.33	127.3
Frequency (Hz)	0.0820	0.0824	0.3317

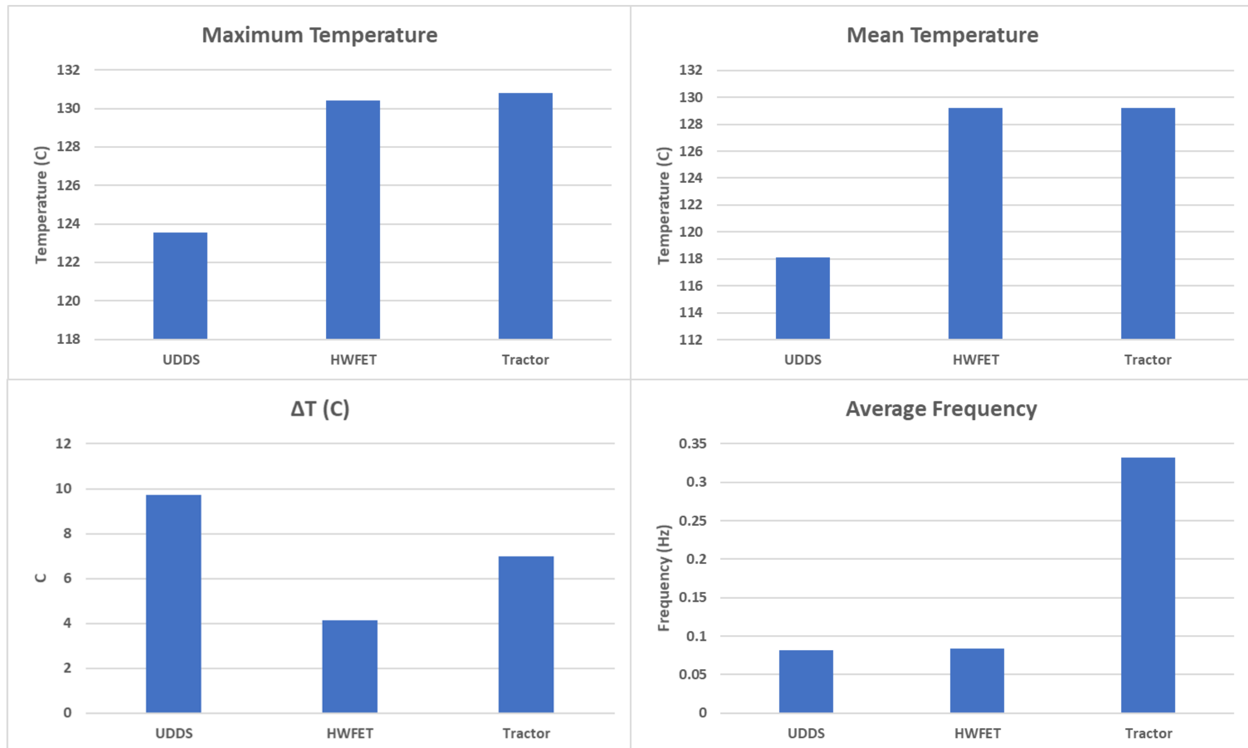

Figure 23. Mission profiles compared for significant reliability factors

Fig. 23 visualizes the key reliability stressors. UDDS does have slightly smaller maximum and mean temperatures, as discussed earlier, but it also has the highest temperature swing, which often plays a greater role in failure than maximum temperature. The tractor drive schedule results in the largest frequency.

4.3.3 Reliability Assessment and Comparison

The lifetimes are predicted using the Norris-Landzberg correlation combined with Miner's Rule. The process is outlined as follows:

Step 1. Parse the temperature profile for cycles. Cycles are defined based on consecutive local maxima and minima.

Step 2. Extract the damage parameters for the cycle.

Step 3. Use the linearized Norris-Landzberg and Held correlations to calculate the cycles to failure.

Step 4. Use its reciprocal to calculate the life consumed (LC) by that cycle.

$$\mathrm{LC} = \frac{1}{N_f} \tag{4}$$

Step 5. Repeat steps 1-4 for each cycle to compute the cumulative damage or consumed life. Failure is predicted when the cumulative damage reaches 1.

$$\mathrm{LC} = \frac{1}{N_1} + \frac{1}{N_2} + \frac{1}{N_3} + \cdots + \frac{1}{N_k} \tag{5}$$

The predicted lifetimes of the two types of interconnects is given below (Fig. 24 (a) and (b)).For both types of interconnects, HWFET results in the longest useful life, followed by tractor drive cycle, while UDDS is predicted to result in the shortest life. This is not entirely surprising, as UDDS is designed to mimic urban driving which is known to cause more wear-and tear in cars. Highway driving, which HWFET is designed to represent, is typically considered as being less demanding of the vehicle. The tractor drive schedule is in between UDDS and HWFET, but is closer to UDDS in its predicted lifetime.

While this is useful, this kind of reliability assessment would be even more insightful if they can be predicted in-situ, for example, if the information could be processed by the car's electronic control unit (ECU) based on sensor inputs in real time. In that situation, however, it may be necessary to truncate the data in order to cut down on computational time and resource.

4.3.4 Characterizing effective frequency and effect on reliability and computational effort

So far, in this study, the temperature profile has been fed into the reliability model and all the peaks and valleys are considered in the reliability quantification. Although, this may be a reasonable

approach when the dataset being analyzed is relatively small, many operating conditions warrant the consideration of damage accumulation in smaller power variation circumstances, including having value in realizing in-situ condition monitoring.

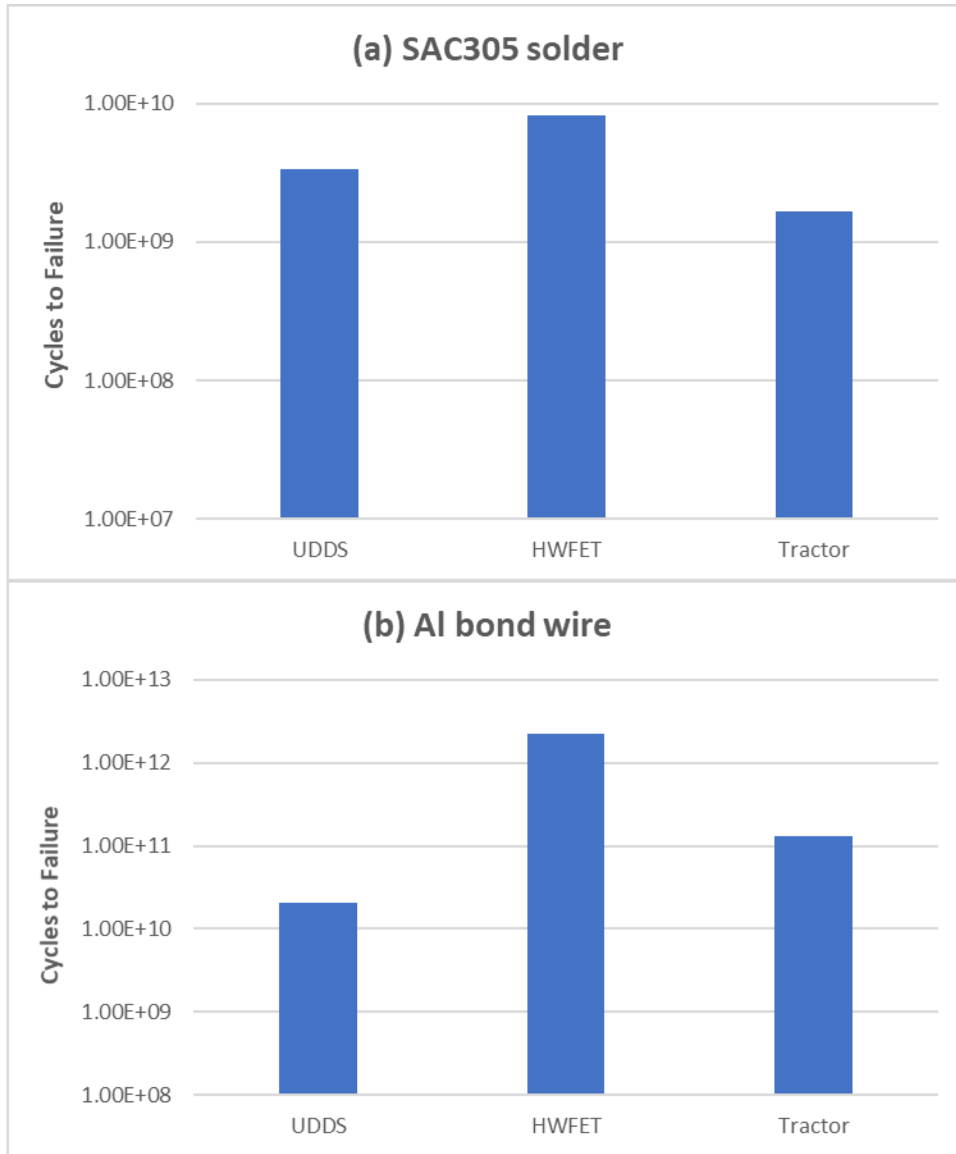

Figure 24. Predicted life for solder balls and Al bond wires for the three different mission profiles

The threshold cycle amplitude is a minimum amplitude that a mini-cycle should have in order for it to be considered as damage inducing. If the temperature swing in the cycle is small, then its

contribution to cumulative damage is also small. The idea here is that if it is small enough, its effect can be ignored without significant increase in error. This results in a decrease in the number of computations required to calculate cyclic damage as well as cumulative damage.

The following sensitivity study was carried out for UDDS mission profile that relates the threshold as a fraction of mean temperature, and the predicted life for SAC305 solder joints (Fig. 25). "Deviation" here is defined as the discrepancy with the initial baseline value obtained by comprehensive cycle counting, which was calculated based on all the cycles. It shows that low deviation can be maintained while still reducing computations significantly in this way. For example, setting a threshold of 0.00002 (or 0.002%) reduces computations by almost 3.4%, but results in deviation less than 1%. Same is true for the other two drive schedules in this study (Figure 26 a, b).

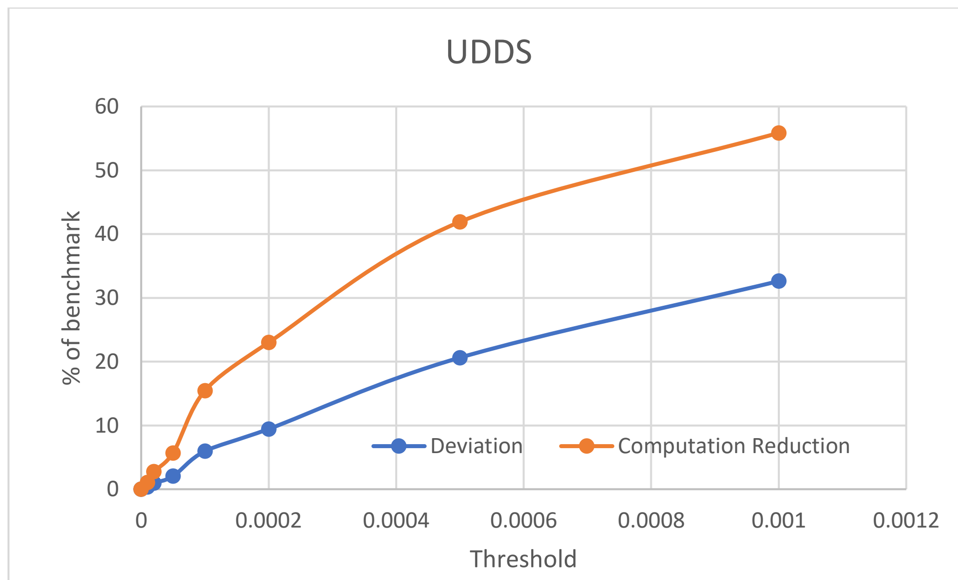

Figure 25. Stability and number of computations for UDDS and agricultural tractor mission profiles

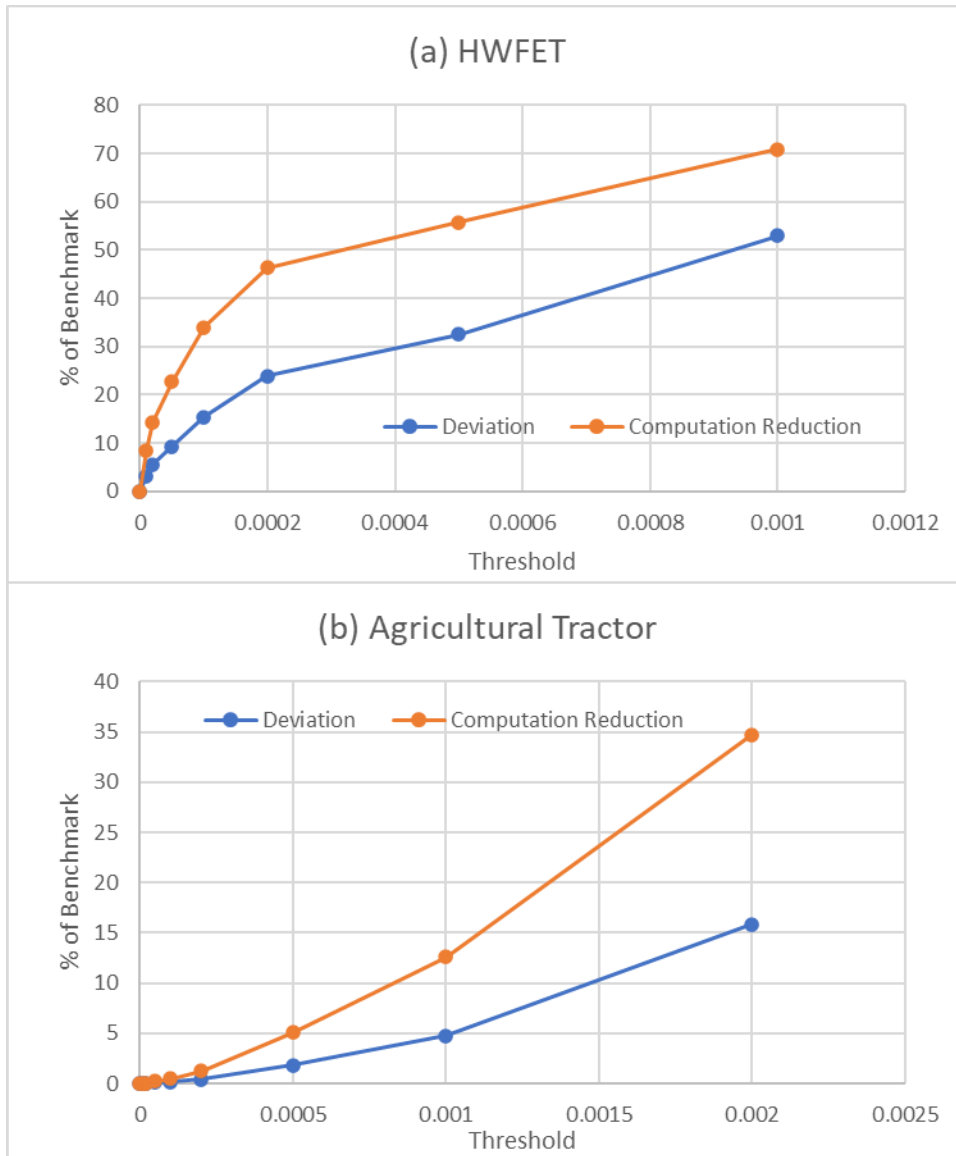

Figure 26. Stability and number of computations for HWFET and agricultural tractor mission profiles

Even though they all show low deviation with computation reduction, there are some differences that are also seen. The UDDS and HWFET drive schedule show that the gradients of the deviation and the computation reduction curves have comparable gradients at larger threshold values, but the tractor drive schedule still shows a sharper slope in the computation reduction curve compared

to the deviation, which suggests that further optimization is possible. The difference possibly arises from the feature of the cycles. The tractor drive schedule has higher number of cycles of small temperature swings, which results in more of these cycles falling below the threshold.

In order to minimize the computational effort in handling such large datasets, it is necessary to find ways to reduce data or computational operations. One way that can be achieved for reliability monitoring of vehicles is by introducing the idea of a threshold cycle amplitude.

4.4 Summary and Conclusions

In this chapter, the model developed in the previous chapter was used to predict temperature profiles based on different mission profiles. Three different mission profiles were analyzed as representative of different driving conditions. They are UDDS (city driving), HWFET (highway driving) and tractor (off road equipment). In order to make the mission profiles relevant in context, they were scaled to the specifications of an actual inverter. The drive schedules were also divided into parts pertaining to startup/shutdown and continuous operation.

The temperature profiles were then used to obtain the damage parameters, such as the mean and maximum temperatures, the temperature swing, and the effective cycling frequency. The thermal transients were found to be very significant for the power modules, which contain the chips dissipating heat, but were significantly less steep for other components, due to the design as well the higher thermal capacitance of the materials used to make them. UDDS has slightly smaller maximum and mean temperatures than HWFET and tractor, but it shows the highest temperature swing, which often plays a greater role in failure than maximum temperature. The tractor drive schedule results in the largest frequency.

The temperature profiles and the extracted parameters were then used to obtain the reliability in terms of cycles to failure. Reliability of two different types of interconnects were compared: SAC solder and Al bond wires. Norris-Landzberg and Held model, respectively, were used along with Miner's rule for damage accumulation. For both, predicted reliability of HWFET was found to be highest, which is expected as has more uniformity than the other two drive schedules.

A sensitivity study was carried out to see the validity of a data reduction technique in reliability computation. It relied on setting a minimum temperature swing for a mini-cycle to be assumed contributory to cumulative damage. The results obtained are promising, with evidence to suggest that data can be significantly reduced while retaining good fidelity. For the UDDS drive schedule, computational time could be reduced by 30% while maintaining less than 10% deviation from benchmark. Similarly, for HWFET and agricultural tractor drive schedule, the computations could be reduced by 23% and 35% respectively while maintaining deviation at less than 10%.

4.5 References

1. https://www.epa.gov/vehicle-and-fuel-emissions-testing/dynamometer-drive-schedules

2. Lau, John H. "Solder joint reliability of flip chip and plastic ball grid array assemblies under thermal, mechanical, and vibrational conditions." *IEEE Transactions on Components, Packaging, and Manufacturing Technology: Part B* 19.4 (1996): 728-735.

3. Norris, K. C., and A. H. Landzberg. "Reliability of controlled collapse interconnections." *IBM Journal of research and Development* 13.3 (1969): 266-271.

4. Arnold, Joelle, et al. "Reliability Testing of Ni-Modified SnCu and SAC305, Accelerated Thermal Cycling." *Resistor* 1.1 (2008): 1.

5. Yang, Guang. *Life cycle reliability engineering*. John Wiley & Sons, 2007.

6. Held, M., et al. "Fast power cycling test of IGBT modules in traction application." *Proceedings of second international conference on power electronics and drive systems*. Vol. 1. IEEE, 1997.

7. Chen, Nian-Zhong, Ge Wang, and C. Guedes Soares. "Palmgren–Miner's rule and fracture mechanics-based inspection planning." *Engineering Fracture Mechanics* 78.18 (2011): 3166-3182.

Chapter 5. System-Level Thermal Management and Reliability of Automotive Electronics: Goals And Opportunities Using Phase Change Materials

Bakhtiyar Mohammad Nafis*, Ange-Christian Iradukunda, David Huitink

Department of Mechanical Engineering,

University of Arkansas, Fayetteville, Arkansas 72701, USA

*Email: *bmohamma@uark.edu*

5.1Abstract

Electronic packaging for automotive applications are at particular risk of thermomechanical failure due to the naturally harsh conditions it is exposed to. With the rise of electric and hybrid electric vehicles (EVs and HEVs), combined with a desire to miniaturize, the challenge of removing enough heat from electronic devices in automotive vehicles is evolving. This paper closely examines the new challenges in thermal management in various driving environments and aims to classify each existing cooling method in terms of performance. Particular focus is placed upon emerging solutions regarded to hold great potential, such as phase change materials (PCMs). Phase change materials have been regarded for some time as a means of transferring heat quickly away from the region with the electronic components and are widely regarded as a possible means of carrying out cooling in large scale from small areas, because of their high latent heat of fusion, high specific heat, temperature stability and small volume change during phase change, etc. They have already been utilized as a method of passive cooling in electronics in various ways, but their adoption in automotive power electronics, such as in traction inverters, has yet to be fulfilled. A brief discussion is made on some of the potential areas of application and challenges relating to

more widespread adoption of PCMs, with reference to a case study using computational model of a commercially available power module used in automotive applications.

Keywords: thermal management, automotive, phase change materials, power electronics

Nomenclature

h	convection coefficient, W/(m^2.K)
E	energy, J
k	thermal conductivity, W/(m.K)
Q	power, W
R	Boltzmann constant
T	temperature, K
z	length along vertical axis, m

Subscripts

f	fusion
m	melting
A	activation

5.2 Introduction

A dramatic shift in electronics cooling requirements in vehicles has occurred during the last two decades, particularly with the advent of electric and hybrid electric vehicles. The most expensive electronic components in cars are no longer GPS and infotainment devices, but rather the powertrain electronics that are central to vehicle propulsion. The semiconductor devices used in

electrical power control systems, such as DC to AC inverters for electric motors and DC to DC converters for powering the accessories, can collectively dissipate power in the range of tens of kilowatts [1]. Traditionally, air cooling has been adequate for automotive electronics, but at these high dissipation rates alternative solutions are required. Existing approaches to cooling these semiconductor devices have utilized liquid coolant loops (typically with a max temperature around 70°C), and some have proposed using vehicle radiator coolant at up to 105°C, however, this is currently problematic for many electronic components which are rated at temperatures below 125°C. Apart from this engine coolant approach, integrating additional cooling systems add considerable cost, weight and volume to a hybrid vehicle drive system, and hence there is a significant need for alternative low-cost, high-performance cooling approaches. As a comparison, Table 10 shows the cooling performances of possible solutions in improving the convective heat transfer coefficient, h, and thereby reduce the coolant system cost through reduced flow requirements and increased temperatures.

The major drawback of these methods, particularly those with the highest performances, is that they are for the most part, liquid-based active methods – in some cases, requiring complex pumping and channeling networks, which adds to the cost and make them susceptible to failure. Alternatively, the use of phase change materials can be an interesting alternative in vehicle systems. Phase change materials work by absorbing heat from the surroundings to first rise to its phase change temperature, then undergoes phase change at constant temperature while absorbing heat. That way, heat continues to be taken in by the PCM, but without causing any temperature rise, at least until all the PCM is melted. In that situation, it has to be allowed to return to its original phase before being used again. Several phase change materials have been investigated, such as *n*-eicosane and other paraffins, sugar alcohols like sorbitol and erythritol [9-12], and there have been

successful attempts to improve their heat transfer characteristics by enhancing them with nanoparticles [13-15]. Low melting point metals, such as Fields' metal, has been explored and found to provide better temperature rise than organic PCMs in some circumstances [16]. Other metals were subsequently studied and found to be able to maintain their properties during long-term reuse [17]. There have also been recent efforts that aim to determine the optimum fin shapes and arrangements that provide best performance when they are used in conjunction with PCMs. Different pin-fin configurations were found to be optimum for different situations: when PCMs are used, staggered pin-fins perform best and when no PCM is used, inline arrangement performs best [18, 19].

Despite advancements, PCMs are yet to take off as a viable cooling solution for automotive applications, and studies have primarily considered mobile, handheld device applications [20, 21]. PCMs do have certain advantages when it comes to automotive electronics cooling. The thermal profile of a drivetrain electronic device is subject to the driving conditions, and therefore is often characterized by fluctuations and sharp peaks. For the Urban Dynamometer Drive Schedule (UDDS), a commonly used drive schedule used by the Environmental Protection Agency, the peak power during which is as much as three times the average power, and the resulting thermal profile has sharp temporary spikes [22]. PCMs, with their ability to absorb heat energy at a constant temperature, is well suited for cooling for such an application [23].

This paper aims to make the case for the adoption of PCMs by highlighting its benefits that can be leveraged in transportation applications – particularly in electric automobiles. Power pulses are used to evaluate the viability of PCM supplemental cooling on a section of a power module used in automotive inverters. Actual drive cycles often involve sharp power peaks many times greater than the average power of the cycle, and therefore power pulses represent the part of the drive

schedule that is most likely to exceed the cooling system dissipation capability temporarily in undersized cooling loops. A detailed resistor network model is analyzed, and specific recommendations are made for the optimum utilization of PCMs in such automotive electric drive applications.

Table 10. Cooling methods and associated heat transfer coefficient ranges.

Cooling method	Type	Effective ‘h’ range ($kW/m^2.K$)
Air cooling [2]	Active	<0.7
Heat pipe [3]	Active/Passive	<14.1
Immersion/boiling [4]	Active	3.8-38.5
Indirect fluid cooling (Single/two phase) [5]	Active	<73.2
Spray cooling [6,7]	Active	<86.0
Jet impingement [8]	Active	5-96.2

5.3 Computational method and FEA validation

Before carrying out computational simulations, the model is validated in two stages to check the accuracy of results. The modeling activity is carried out using ParaPower, an open source tool developed by the Army research Lab (ARL) that solves a resistor network (RN) model of the system using implicit Euler formulation [24, 25]. It is a streamlined, MATLAB-based code that

offers fast analysis of thermo-mechanical systems, and incorporates a medium fidelity modeling capability for phase change materials.

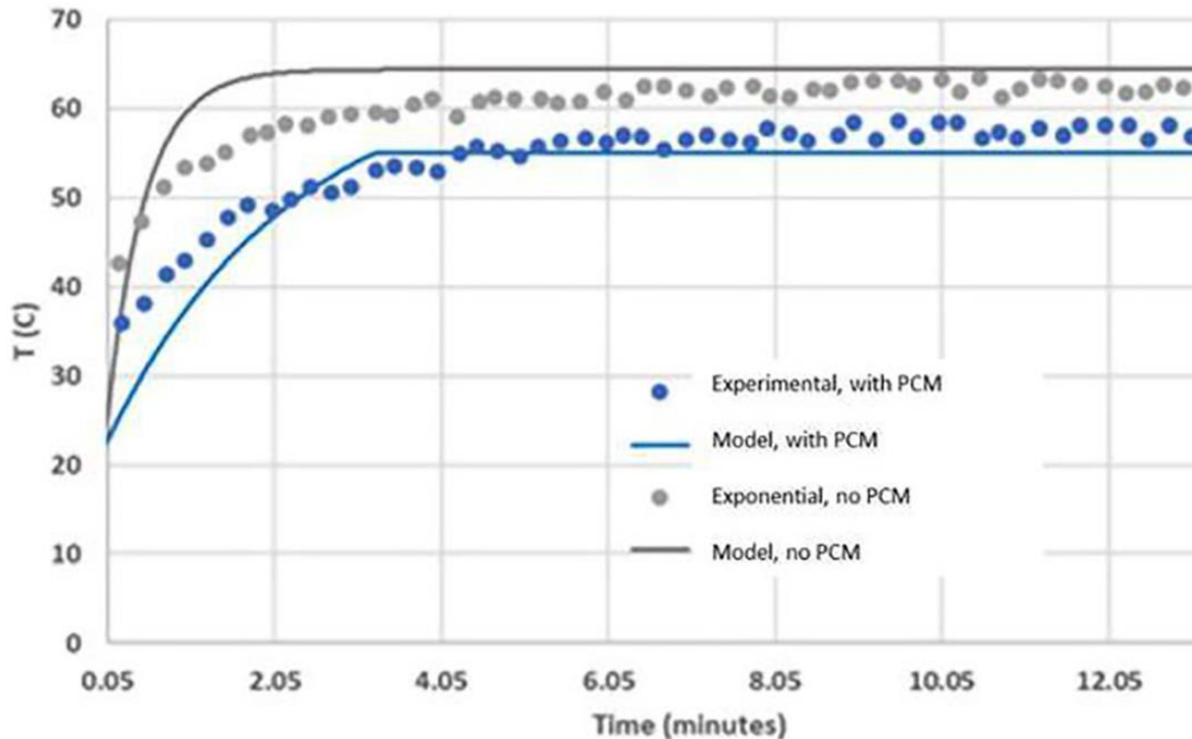

Figure 27. Comparison of model with experimental results from Kandasamy et al. [26]

For the first stage, ParaPower results were compared with published experimental data, where Kandasamy, Wang and Mujumdar [26] carried out experimental work with paraffin wax as the PCM embedded in finned heat sinks with three different heat sink geometries. The results for one such heat sink, termed HS1 by the authors of that paper, with Q = 2 W was compared to the ParaPower RN model (Fig. 27). The model shows considerable agreement with experimental results in terms of the temperature rise. The final temperature predicted by the model are within 20 C of the experimentally obtained values for both PCM and no PCM cases. The discrepancy in time to reach steady state is attributable to the simplifications introduced in the model, such as the assumption that heat transfer takes place only through the heat sink and ignoring other losses which

would be present to some extent in an actual experiment. For thermal analysis purposes, the mathematical model is concluded to have sufficient accuracy for use as a tool for further analysis.

In the second stage of validation, a power module was modeled based on a commercially available insulated-gate bipolar transistor (IGBT) module. The IGBT power module is commonly used in electric and hybrid electric vehicle inverter systems and thus was used as a reference configuration for device placement and package architecture (segment shown in Fig. 28). Given the type of IGBT and voltage current ratings currently employed in automotive traction systems, these internal die placements are representative of many other power modules used in EV and HEV inverters. The section represented in Fig. 28 is a reduced subsection of a complete module with two switches (IGBT) and two diodes, in order to facilitate faster computation on repeated components in the actual power package. The IGBT chips are each 4 mm by 6 mm with a height of 0.25 mm. For thermal dissipation modeling, the module section is attached to an appropriately scaled finned heat sink containing PCM (Xylitol), as shown in Fig. 29, and simulations are carried out in both ANSYS Fluent and ParaPower for comparison, with a constant heat load. The heat sink, which was modeled as similar to the one used by Kandasami et al., [26] was characterized in terms of the thermal resistance between the base and fin tip to make the approach as generic as possible.

In order to establish the validity of the model, and to ascertain the appropriateness of ParaPower in this context, a constant power of 2 W was used to compare the results of PCM thermal performance in both ParaPower and ANSYS Fluent. Xylitol was chosen as the evaluation PCM in this study for its fairly large latent heat (ΔH_f=300 J/g) and melting temperature (Tm=94°C) which may be optimal for maintaining electronics temperatures below commonly rated junction temperatures of $T_{j,max}$=125°C. Table 11 compares the maximum stable temperature and the melt fraction of the Parapower model with the ANSYS Fluent model. The results were taken after 30

minutes of simulated time, at which point the temperature had attained stable values. The melt fraction shows all PCM to have melted, which is consistent with the peak temperature values shown in Table 11.

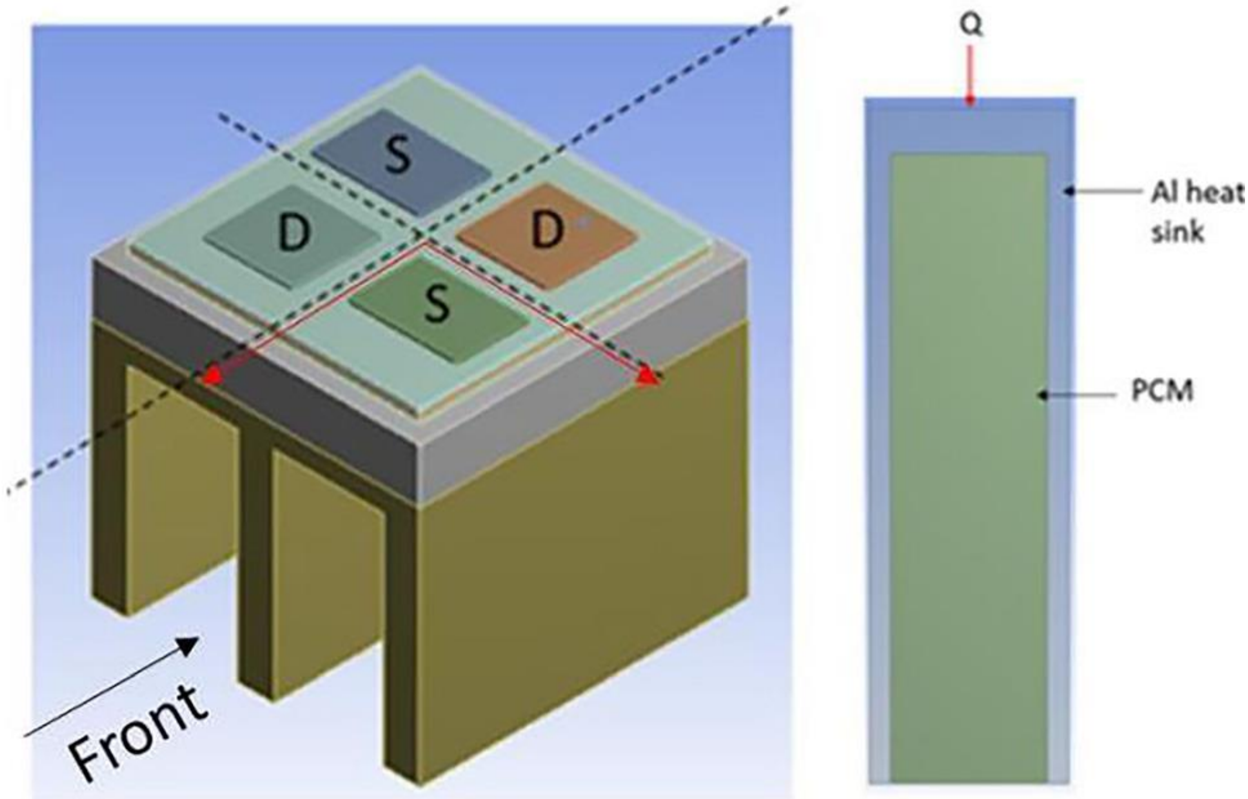

Figure 28. Model of power module unit with dotted section lines (left) and two-dimensional section used for CFD (ANSYS) model, with direction of heat flux indicated

Table 11. Results obtained from ParaPower compared to results from ANSYS, showing the maximum die temperatures and PCM melt fractions for a benchmarking case study.

	ParaPower	ANSYS Fluent
Max. T (C)	147	134
Final Melt fraction	1.0	1.0

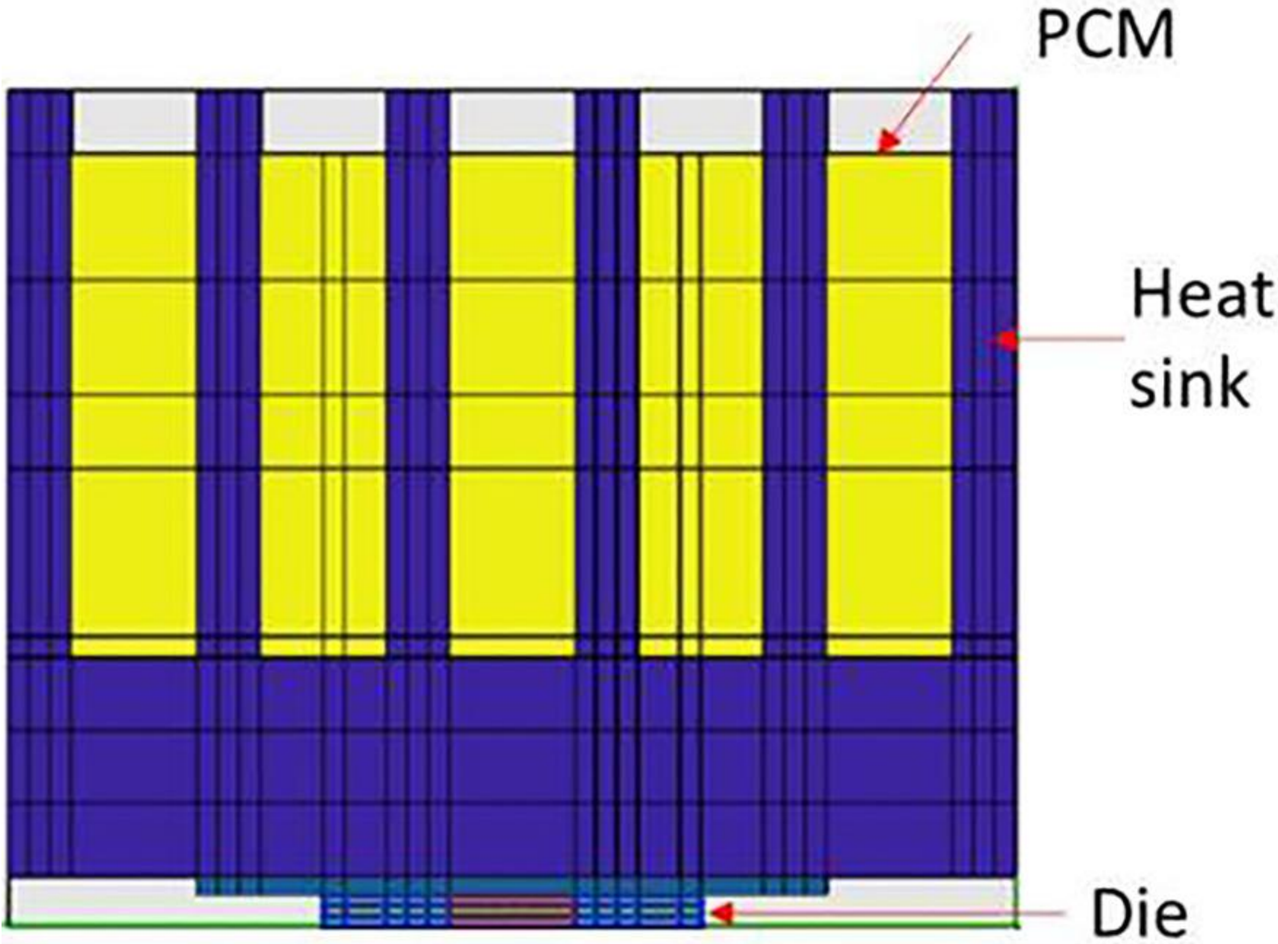

Figure 29. PARAPOWER computational model of a heat sink geometry with the PCM between fins for comparison with experimental results

As noted in the table, the maximum temperature obtained from ParaPower was predicted to be higher than that modeled in ANSYS. This discrepancy is due to the simplified, two-dimensional simulation considered in ANSYS, and because ParaPower only considers conduction in the PCM while ignoring the bulk motion of a liquefied species. In reality, there is likely to be some flow behavior when the PCM is in liquefied state, arising from natural convection. As reported by the ARL creators, this difference is expected, and for the sake of rapid optimization exercise, the results agree well enough (within 11%) that ParaPower can be used to provide a more conservative analysis for sensitivity study, such that its rapid calculation protocol can aid in parametric thermal analysis.

Having established reasonable fidelity in the ParaPower tool, it can serve as a helpful aid in performing rapid, thermal sensitivity studies for PCM integrated cooling. In order to parametrically analyze the module's thermal performance, the load, convection coefficient and the PCM amount (which concurrently affects the associated thermal resistance) was varied. Since latent heat activity is proportional to the mass (or volume) of the PCM, the PCM latent heat absorption sensitivity analysis was accomplished via adjusting the vertical length (along the z-axis) of the heat sink. As the heat sink is filled with PCM, it results in differing PCM mass content. The computational model used is the same as in Fig. 29. A convection boundary condition was applied at the top surface of the PCM-heat sink, so the fin tips and the top surfaces of embedded PCM are exposed to convection. The heat loads were taken to be power pulses of different magnitudes lasting 10 seconds, and the initial temperature of the system was taken to be at just below the melting temperature of the PCM (94 °C for Xylitol). Under this assumed condition, the additional incoming thermal energy goes into the phase change process rather than temperature rise associated with the specific heat of the solid. A power dissipation curve for an automobile

typically has sharp peaks that are often many times greater than the average power, and these peaks pose the biggest thermal management challenge. A pulsed power study, consisting of short duration dissipation events followed by a cool down period (no power, but cooling activated), can therefore be used to simplify automotive power load in a square wave function that can represent an extreme case of what is to be handled by the cooling system. The following parameters tested are listed in Table 12.

Table 12. Conditions analyzed during simulation activity.

Parameter	Range analyzed
Convection coefficient (h), $W/m^2.K$	5 - 80
Pulse magnitude, (Q_{pulse}), W	1 - 4
Heat sink-PCM vertical length (z), mm	5 – 17.5

5.4 Results and discussion

With the application of power pulses, the entities with and without PCM both experience varying temperature rises, but the total energy absorbed to raise the temperature would be small in case of a simple heat sink (no PCM) compared to when a PCM is present. Addition of PCM has several effects. It adds mass to the system, so the overall heat capacity of the heat sink-PCM configuration is higher. The PCM usually has a much lower thermal conductivity and introduces a high latent heat. The result is an interplay between multiple thermal phenomena: heat absorbed by PCM

during phase change, increased heat capacity of system, reduction in convective heat transfer area due to introduction of PCM and changes in the thermal resistance from die to coolant.

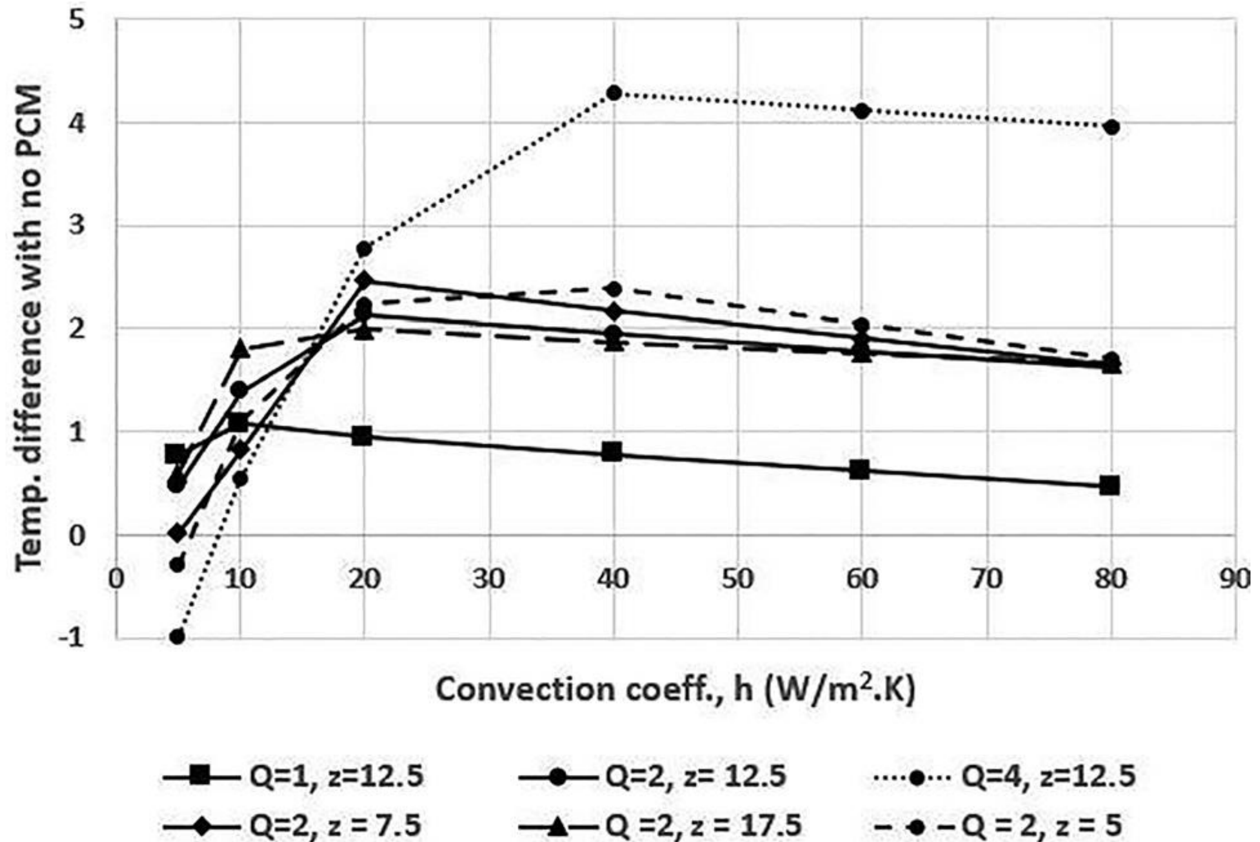

Figure 30. Temperature difference between PCM and no-PCM condition with convection coefficient (h) at different pulse magnitudes (Q) and PCM-heat sink height (z)

The adoption of PCM is associated with concerns about its performance when compared to that of heat rejection mechanisms without PCM, such as air cooled heat sinks. It is therefore necessary that the PCM case is compared directly with a no PCM case. Fig. 30 shows the temperature difference between the two cases. Different fin heights (z), pulse magnitude (Q) and convection coefficients (h) were considered, but for compared cases those variables were held constant. The ordinate values are the die temperatures for a PCM case subtracted from the temperature for the corresponding no PCM case. It can be seen that for a wide range of convection coefficients,

introduction of PCM actually results in a higher die temperature – due to the added thermal resistance of the organic PCM studied (Xylitol, k=0.5 W/mK). Only when the 'h' values are less than 10 W/m^2K, the PCMs show temperature advantage over a typical heat sink (no PCM) of similar geometry (negative values). There are only two data points that show PCM integration resulting in a lowering of the maximum die temperature compared to the heat sink working alone, and they were obtained in the region where h<10. In Fig. 31 the data is presented in terms of the effective thermal resistance for a single pulse condition of only Q = 2 W for 10 seconds. Herein, the results indicate that the most beneficial case for PCMs are for those situations that create little additional thermal resistance, and their activity is maximized where the convective heat removal is significantly limited. In other words, PCM performance can be improved through increasing the conductivity of the PCM in a geometric configuration where convection is not driven significantly by the PCM surface area.

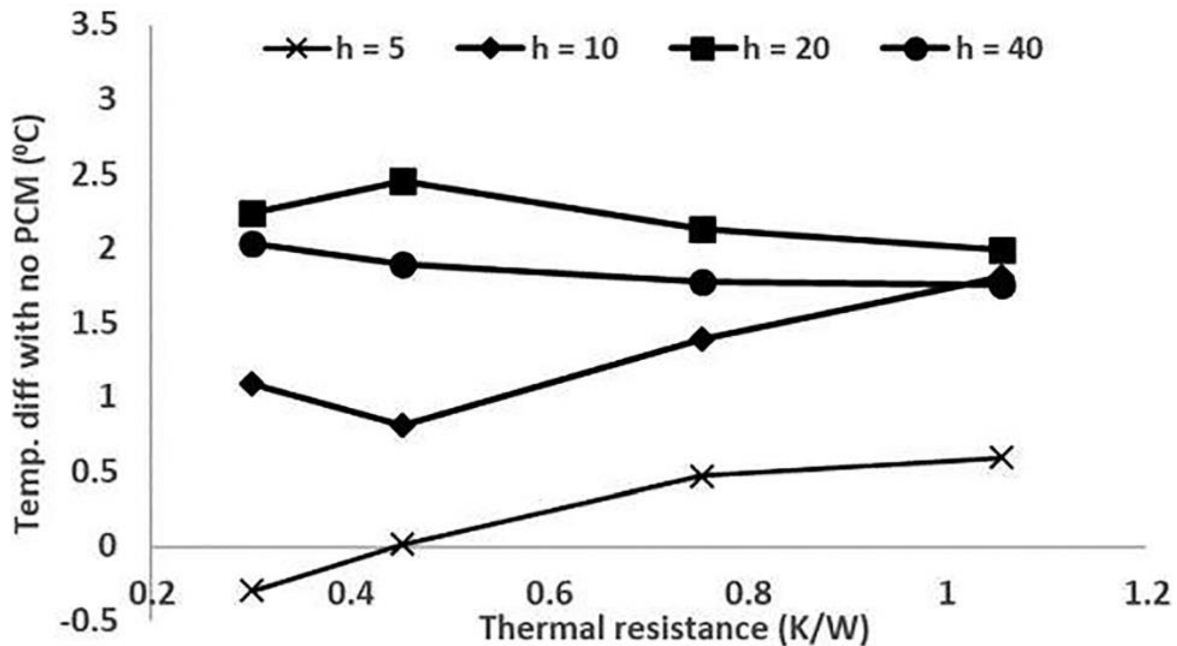

Figure 31. Maximum die temperature rise with the thermal resistance, for Q = 2W

5.5 Reliability consideration

Of course, temperature management in electronics is merely a means to achieve reliable performance, and temperatures only matter insofar as the devices and packaging can operate according to expectations. As such, the reliability of the electronic equipment is a critical consideration in designing a thermal management scheme. Moreover, the application of PCM holds great promise for its ability to mitigate peak temperatures from transient power loads if properly incorporated; but if PCMs raise the peak temperatures through added thermal resistance, it may further accelerate thermally aggravated failure modes.

Interconnect failure often represents the highest failure risk in power electronics, due both to the regularity and criticality of interconnect failure. For example, an attempt to study the reliability of insulated-gate bipolar transistors (IGBT) devices for traction applications consistently found the first failure to be always at the aluminum wire bonds, an interconnection often used in electronic packaging [28]. As the wirebonds were always the first to fail, the model should apply to other types of modules, such as metal oxide semiconductor field effect transistors (MOSFETs) that use aluminum wire bonds. Given the lifetime dependency on temperature on wirebond life as observed by Held et al. [28], (expressed in Eq. (1)) this correlation can be used to help describe the potential reliability benefit (or detriment) when considering PCM integration.

$$N_L = A(\Delta T)^{-5} e^{-\frac{E_A}{RT}} \quad (1)$$

Here N_L is the number of cycles to failure, ΔT is the temperature swing, R is the Boltzman constant and T is the midpoint temperature within the cycling range. For aluminum wirebonds, Held et al. reported, coefficient A=6400, E_A= 78000 J. Using this relationship, and based on temperature data presented in Fig. 30, the corresponding improvement (or degradation) in reliability when PCM is

used is presented in Fig. 32. The reliability index, on the ordinate, is the ratio of lifetime (in no. of cycles to failure) for PCM to the no-PCM case. As with the temperature reduction results formerly, only two data points demonstrated a reliability index greater than one. For each case represented by a curve, the best reliability indices are predicted in case of low convective heat transfer coefficient, especially when the heat transfer coefficient is smaller than 10 W/m^2K.

5.6 Implication for cooling system design

Beyond purely abating peak temperatures for reliability enhancement, another key aspect of ensuring prevention of excessively high die temperatures is the regeneration (i.e. return to solid form) of the PCM material so that it is ready to be used in the next power dissipation pulse or temperature excursion. One added complication is that, even at the same average power, an intense power peak can cause a thermal bottleneck situation, leading to potential damage to the electronics. This is shown in Fig. 33. Here the same average power is applied over 20 seconds, but results in slightly different solidification times. As a result, thermal management design should consider both peak power and the average power.

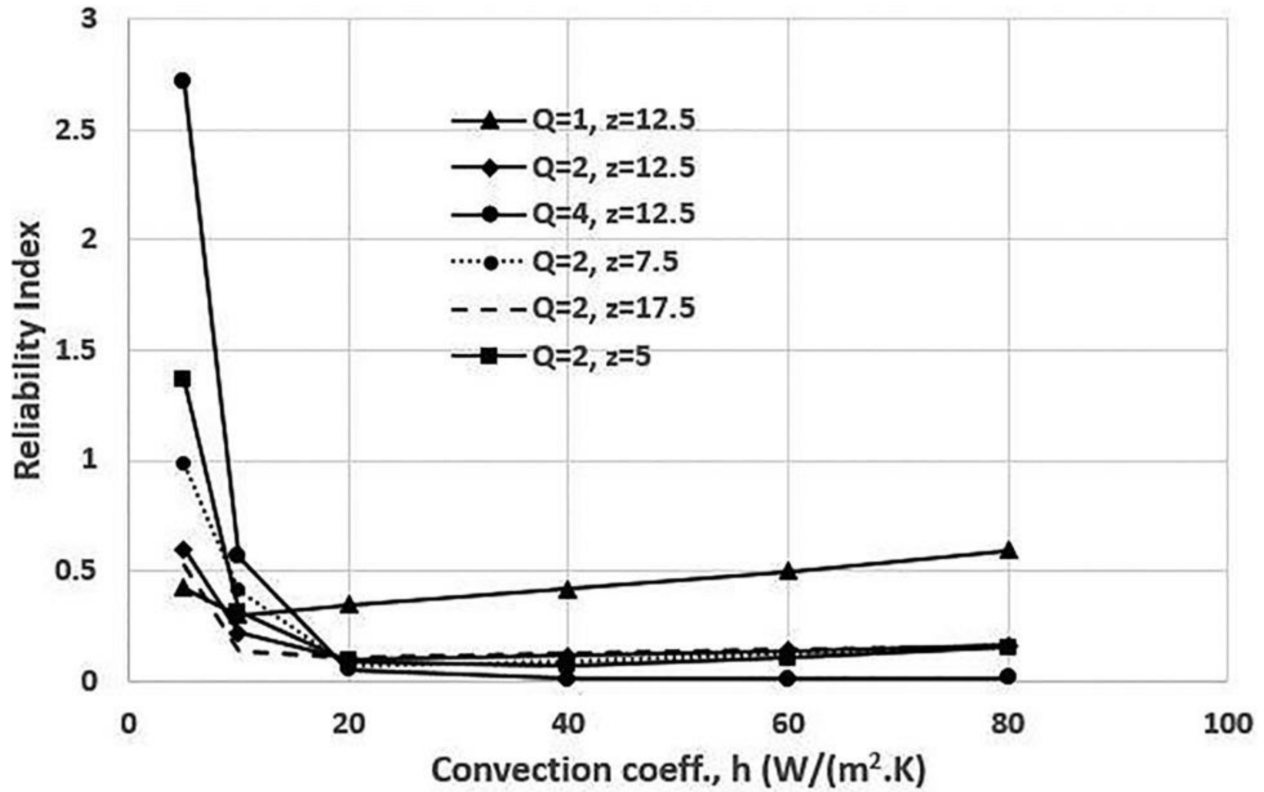

Figure 32. Reliability index with h, at different peaks and heat sink sizes

For example, Fig. 34 illustrates the maximum average power (the highest average power level over a prescribed time period) that the system can safely and continuously handle. The pulse here is 2 W in either case, and the maximum average power is seen to be heavily influenced by the cooling method and heat sink efficacy (in terms of z-height here). The regeneration time (i.e. time needed for the molten PCM to re-solidify completely) is also shown on the same chart. Because the power handling capability changes with the peak power, any safe operation envelope must consider peak, average power, cooling method and PCM amount (i.e. thermal capacitance) and/or the resulting thermal resistance.

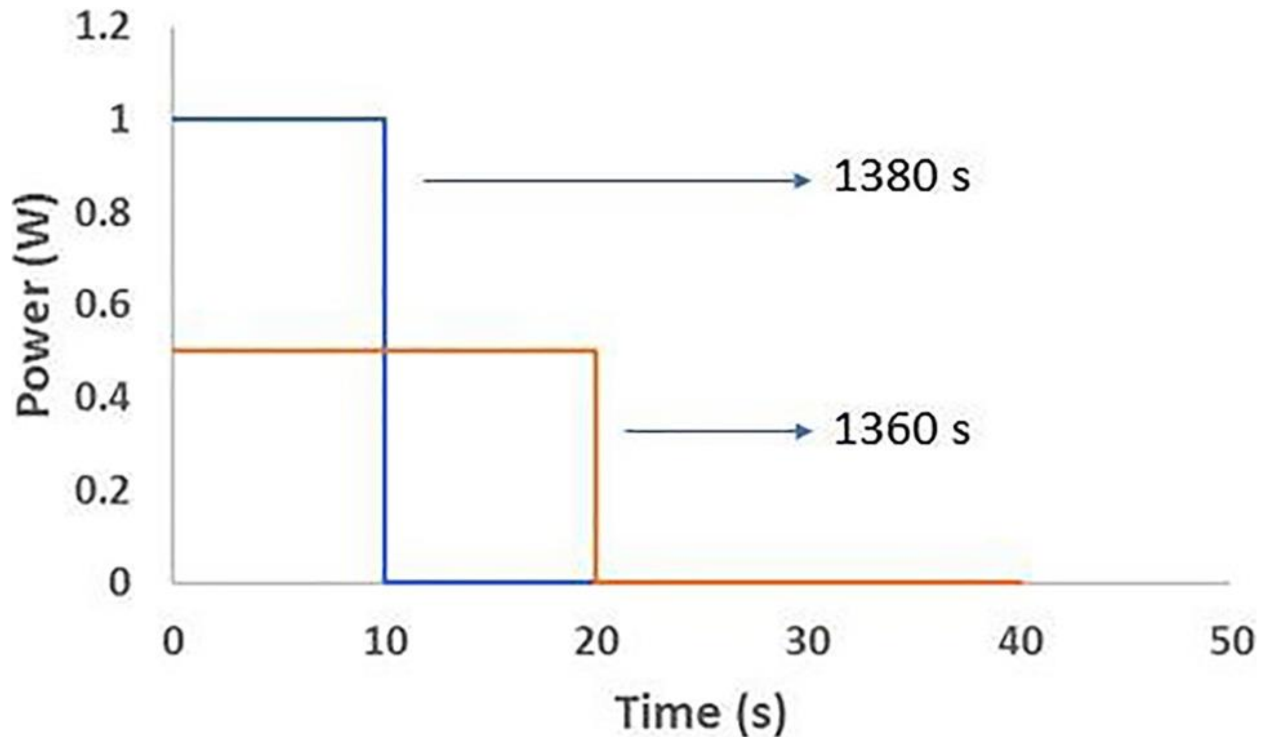

Figure 33. At same average power, different peak magnitudes result in different regeneration times due to thermal bottlenecks

Fig. 34 shows the maximum average power (circles, primary axis) and the regeneration times (squares, secondary axis) for different values of z and h for a single die. While it does clearly show enhanced power handling capability and faster regeneration at higher convection coefficients, the system as a whole would not necessarily be useful as its thermal performance would be inferior to that of a simple (no PCM) heat sink. This indicates that PCM integration is most useful in situations corresponding to the left end of the chart in Fig. 34, where the convection coefficient (h) is less than 10 W/m^2K and a thinner PCM layer would give the most promising result because of its shorter regeneration time. Of course, this also implies that the optimized PCM layer thickness will be specific to the geometry of the system and the thermal properties of the selected PCM. The design considered in this study favors a thinner layer because the area of contact between fluid and PCM is small, and all thermal energy must pass through the PCM-heat sink to reach the coolant.

In this analysis the power levels considered here were small, with a maximum of 2 W over 10 seconds. For greater and longer pulses, other possible design considerations have to be made that will have optimized the system for a thicker PCM layer, which would have greater temperature stabilizing capability. An improved design should also flow some coolant directly over the dies. That would mitigate the problem of increased thermal resistance when PCM is introduced, and so PCM integration would exhibit improvement over a regular heat sink over a much wider range of convection coefficient values.

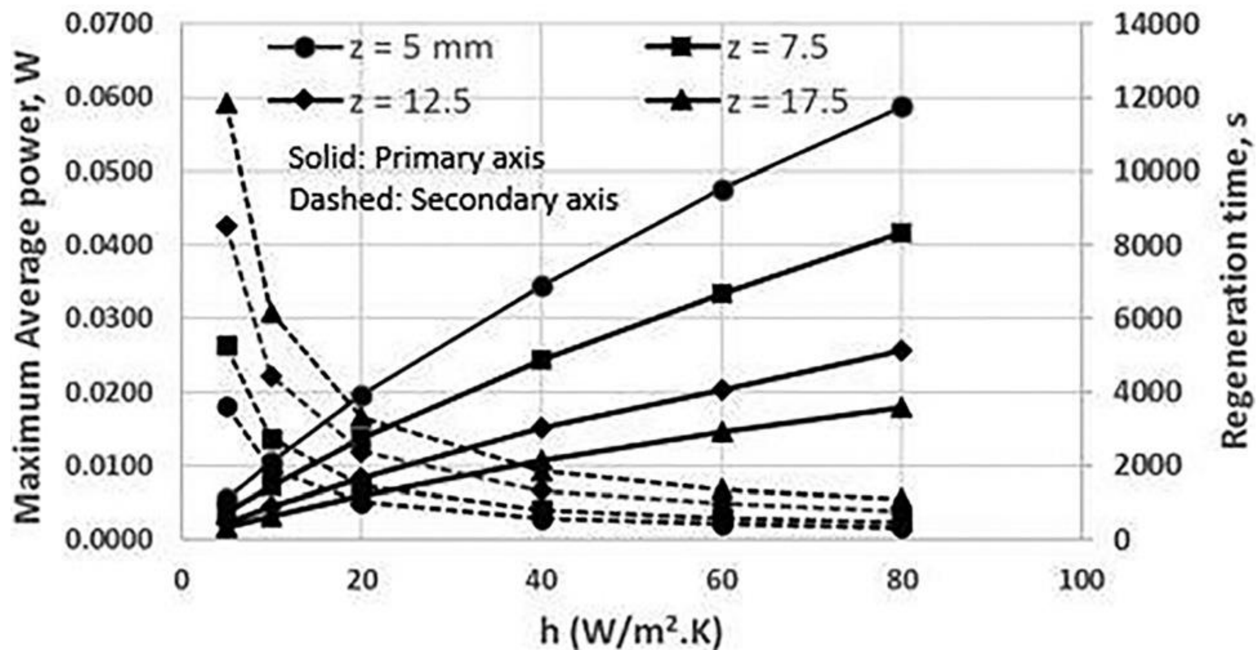

Figure 34. Chart proposing optimum operating envelope for continuous operation

In cases where PCMs are advantageous based on the power profile, the designer in charge of designing a vehicle's cooling system will have to make critical decisions regarding the ratio of cooling load shared between the PCM and a more conventional active cooling system, such as a fan. If the system is designed with a smaller fan, a greater mass of PCM must be stored, which adds weight to the vehicle. A properly optimized system would ensure that a large fraction of the

PCM is liquefied during operation, as that implies energy being stored as latent heat. The higher the mass of the PCM packed into the cooling system, the more heat it can store, but a large amount of PCM would add significant weight to the vehicle. Hence, the mass of the PCM, along with operating environment, would also be an important factor in identifying the ideal thermal management scheme. Conversely, directing more energy through convective heat removal may require a larger fan size that would be able to carry away more heat, but besides adding more weight, it will also draw more power from the vehicle's power plant. The decision thus boils down to one between a more passive system (more PCM, lower fan power) and a more active system (more fan power).

5.7 Conclusion

Phase change materials may offer a promising method of cooling electronics in the context of variable power loads, such as those seen in electric vehicle operation, yet there is a delicate thermal design optimization that must be considered. PCMs may help to ensure a more consistent temperature profile by mitigating the peaks by undergoing constant temperature phase changes. They can also facilitate an extra level of control to the thermal engineer as the PCM works like a constant temperature heat sink. Research on PCMs until now have largely focused on consumer electronics, such as mobile devices, but it can bring the same advantages to automotive cooling. Using a computational model to simulate transient temperature distribution, it was shown that using a PCM such as Xylitol can lead to a more consistent temperature profile with lower peaks and smaller temperature swings, under conditions where conduction, convection and latent heat exchange were in the appropriate balance. This in turn can lead to a significant enhancement in useful life of an automotive electronic device. However, the PCM (particularly organic) also increases the thermal resistance from the die to the ambient (or coolant), and thus, for low

conductivity PCMs, utility is best at small convection coefficients (h < 10 $W/m^2.K$) and thin PCM layers. Using a medium fidelity fast modeling approach to PCM thermal management design, an expedient operating envelope was presented for xylitol with a typical, commercially available power module as a case study, and it was shown that both peak load and average load will have to be factored in any design decisions, as well as PCM size and cooling method. This work illustrates the importance of design tradeoffs in electronics thermal management, particularly where automotive power electronics may be concerned; and furthermore, points to the importance of both PCM property enhancement and system integration for realizing passive cooling reliability benefits. Other configurations and materials not considered here may offer greater benefit, but sizing them with the system thermal loads is critical, and thermal designers must consider factors of melt time, re-solidification and material properties in the context of the thermal pulse load and frequency in the design of interest.

5.8 Acknowledgement

The authors would like to thank Dr. Yarui Peng and Imam Al Razi, from the Department of Computer Science and Computer Engineering, University of Arkansas, for helpful discussion and support. The information, data, or work presented herein was funded in part by the Advanced Research Projects Agency-Energy (ARPA-E), U.S. Department of Energy, under Award Number DE-AR0000895 in the CIRCUITS program monitored by Dr. Isik Kizilyalli. The views and opinions of authors expressed herein do not necessarily state or reflect those of the United States Government or any agency thereof.

5.9 References

[1] Myers, Bruce A., Gary Eesley, and David Ihms. "Electronics cooling in the automotive environment." *Electronics cooling* 16, no. 1 (2010): 16-21.

[2] Katoh, Takahiro, Guoping Xu, Marlin Vogel, and Shlomo Novotny. "New attempt of forced-air cooling for high heat-flux applications." In *The Ninth Intersociety Conference on Thermal and Thermomechanical Phenomena In Electronic Systems (IEEE Cat. No. 04CH37543)*, vol. 2, pp. 34-39. IEEE, 2004.

[3] Zimbeck, Walter, Greg Slavik, John Cennamo, Sukhvinder Kang, James Yun, and Edward Kroliczek. "Loop heat pipe technology for cooling computer servers." In *2008 11th Intersociety Conference on Thermal and Thermomechanical Phenomena in Electronic Systems*, pp. 19-25. IEEE, 2008.

[4] Ali, Amir F., and Mohamed S. El-Genk. "Effect of inclination on saturation boiling of PF-5060 dielectric liquid on 80-and 137-μm thick copper micro-porous surfaces." *International journal of thermal sciences* 53 (2012): 42-48.

[5] Bertsch, Stefan S., Eckhard A. Groll, and Suresh V. Garimella. "Effects of heat flux, mass flux, vapor quality, and saturation temperature on flow boiling heat transfer in microchannels." *International Journal of Multiphase Flow* 35, no. 2 (2009): 142-154.

[6] Martínez-Galván, Eduardo, Raúl Antón, Juan Carlos Ramos, and Rahmatollah Khodabandeh. "Influence of surface roughness on a spray cooling system with R134a. Part I: Heat transfer measurements." *Experimental thermal and fluid science* 46 (2013): 183-190.

[7] Martínez-Galván, Eduardo, Juan Carlos Ramos, Raúl Antón, and Rahmatollah Khodabandeh. "Influence of surface roughness on a spray cooling system with R134a. Part II: Film thickness measurements." *Experimental thermal and fluid science* 48 (2013): 73-80.

[8] Browne, Eric A., Gregory J. Michna, Michael K. Jensen, and Yoav Peles. "Microjet array single-phase and flow boiling heat transfer with R134a." *International Journal of Heat and Mass Transfer* 53, no. 23-24 (2010): 5027-5034.

[9] Akgün, Mithat, Orhan Aydın, and Kamil Kaygusuz. "Experimental study on melting/solidification characteristics of a paraffin as PCM." *Energy Conversion and Management* 48, no. 2 (2007): 669-678.

[10] Beemkumar, N., A. Karthikeyan, C. Parthasarathy, and B. Bradley Bright. "Heat transfer analysis of latent heat storage system using D-Sorbitol as PCM." *ARPN Journal of Engineering and Applied Sciences* 10, no. 11 (2015): 5017-5021.

[11] Alkan, Cemil, Ahmet Sarı, and Ali Karaipekli. "Preparation, thermal properties and thermal reliability of microencapsulated n-eicosane as novel phase change material for thermal energy storage." *Energy Conversion and Management* 52, no. 1 (2011): 687-692.

[12] Agyenim, Francis, Philip Eames, and Mervyn Smyth. "Experimental study on the melting and solidification behaviour of a medium temperature phase change storage material (Erythritol) system augmented with fins to power a LiBr/H2O absorption cooling system." *Renewable energy* 36, no. 1 (2011): 108-117.

[13] Liu, Xiaosong, Cody Marbut, David Huitink, Gang Feng, and Amy S. Fleischer. "Influence of crystalline polymorphism on the phase change properties of sorbitol-Au nanocomposites." *Materials Today Energy* 12 (2019): 379-388.

[14] Iradukunda, Ange-Christian, Josh Kasitz, Hayden Carlton, David Huitink, Amol Deshpande, and Fang Luo. "Concurrent Thermal and Electrical Property Effects of Nano-Enhanced Phase Change Material for High-Voltage Electronics Applications." *Journal of Electronic Packaging* 142, no. 3 (2020).

[15] Colla, Laura, Davide Ercole, Laura Fedele, Simone Mancin, Oronzio Manca, and Sergio Bobbo. "Nano-phase change materials for electronics cooling applications." *Journal of Heat Transfer* 139, no. 5 (2017).

[16] Gonzalez-Nino, David, Lauren M. Boteler, Dimeji Ibitayo, Nicholas R. Jankowski, Damian Urciuoli, Iain M. Kierzewski, and Pedro O. Quintero. "Experimental evaluation of metallic phase change materials for thermal transient mitigation." *International Journal of Heat and Mass Transfer* 116 (2018): 512-519.

[17] Báez, Rafael, Luis E. González, Manny X. de Jesús-López, Pedro O. Quintero, and Lauren M. Boteler. "Metallic Phase Change Material's Microstructural Stability Under Repetitive Melting/Solidification Cycles." *Journal of Electronic Packaging* 142, no. 3 (2020).

[18] Arshad, Adeel, Hafiz Muhammad Ali, Shahab Khushnood, and Mark Jabbal. "Experimental investigation of PCM based round pin-fin heat sinks for thermal management of electronics: effect of pin-fin diameter." *International Journal of Heat and Mass Transfer* 117 (2018): 861-872.

[19] Ashraf, Muhammad Junaid, Hafiz Muhammad Ali, Hazrat Usman, and Adeel Arshad. "Experimental passive electronics cooling: parametric investigation of pin-fin geometries and efficient phase change materials." *International Journal of Heat and Mass Transfer* 115 (2017): 251-263.

[20] Tan, F. L., and C. P. Tso. "Cooling of mobile electronic devices using phase change materials." *Applied thermal engineering* 24, no. 2-3 (2004): 159-169.

[21] Ali, Hafiz Muhammad. "Experimental investigation on paraffin wax integrated with copper foam based heat sinks for electronic components thermal cooling." *International Communications in Heat and Mass Transfer* 98 (2018): 155-162.

[22] Nafis, Bakhtiyar Mohammad, Ange Iradukunda, and David Huitink. "Drive Schedule Impacts to Thermal Design Requirements and the Associated Reliability Implications in Electric Vehicle Traction Drive Inverters." In *ASME 2018 International Technical Conference and Exhibition on Packaging and Integration of Electronic and Photonic Microsystems*. American Society of Mechanical Engineers Digital Collection, 2018.

[23] Boteler, Lauren, Michael Fish, Morris Berman, and Justin Wang. "Understanding Trade-Offs of Phase Change Materials for Transient Thermal Mitigation." In *2019 18th IEEE Intersociety Conference on Thermal and Thermomechanical Phenomena in Electronic Systems (ITherm)*, pp. 870-877. IEEE, 2019.

[24] Boteler, L. M., and S. M. Miner. "Power packaging thermal and stress model for quick parametric analyses." In *ASME 2017 International Technical Conference and Exhibition on Packaging and Integration of Electronic and Photonic Microsystems collocated with the ASME 2017 Conference on Information Storage and Processing Systems*. American Society of Mechanical Engineers Digital Collection, 2017.

[25] Boteler, L. M., and S. M. Miner. "Comparison of Thermal and Stress Analysis Results for a High Voltage Module Using FEA and a Quick Parametric Analysis Tool." In *ASME 2018 International Technical Conference and Exhibition on Packaging and Integration of Electronic and Photonic Microsystems*. American Society of Mechanical Engineers Digital Collection, 2018.

[26] Kandasamy, Ravi, Xiang-Qi Wang, and Arun S. Mujumdar. "Transient cooling of electronics using phase change material (PCM)-based heat sinks." *Applied thermal engineering* 28, no. 8-9 (2008): 1047-1057.

[27] Held, M., P. Jacob, G. Nicoletti, P. Scacco, and M-H. Poech. "Fast power cycling test of IGBT modules in traction application." In *Proceedings of Second International Conference on Power Electronics and Drive Systems*, vol. 1, pp. 425-430. IEEE, 1997.

Chapter 6. Conclusions

6.1 Summary

As automotive electronics become a part of the drivetrain itself, their reliability is intricately connected to the reliability of the vehicle itself. To that effect, it is important to study the effect of the mission profile of the vehicle itself on the power electronics reliabilities. However, in order to do that, it is important to identify the differences in the mission profiles that various components are subject to. A way to estimate the mission profiles of the power electronics from the vehicle mission profile is by using a lumped capacitance thermal model where the parameters are approximated based on the physical dimensions and material properties of the system. In this study, vehicle mission profiles from the Environmental Protection Agency were used to derive the temperature profile of the power electronics and other components using lumped capacitances. The model was validated experimentally, and sufficient agreement was found. There were some discrepancy, however, which could be attributed to uncertainties in approximations regarding the internal volume of the cold plate and the surface area subject to convection by the coolant, as well as heat lost to the surroundings.

The temperature profiles were then used to obtain the damage parameters, such as the mean and maximum temperatures, the temperature swing, and the effective cycling frequency. The thermal transients were found to be very significant for the power modules, which contain the chips dissipating heat, but were significantly less steep for other components, due to the design as well the higher thermal capacitance of the materials used to make them. UDDS has slightly smaller maximum and mean temperatures than HWFET and tractor, but it shows the highest temperature swing, which often plays a greater role in failure than maximum temperature. The tractor drive schedule results in the largest frequency.

The temperature profiles and the extracted parameters were then used to obtain the reliability in terms of cycles to failure. Reliability of two different types of interconnects were compared: SAC solder and Al bond wires. Norris-Landzberg and Held model, respectively, were used along with Miner's rule for damage accumulation. For both, predicted reliability of HWFET was found to be highest, which is expected as has more uniformity than the other two drive schedules.

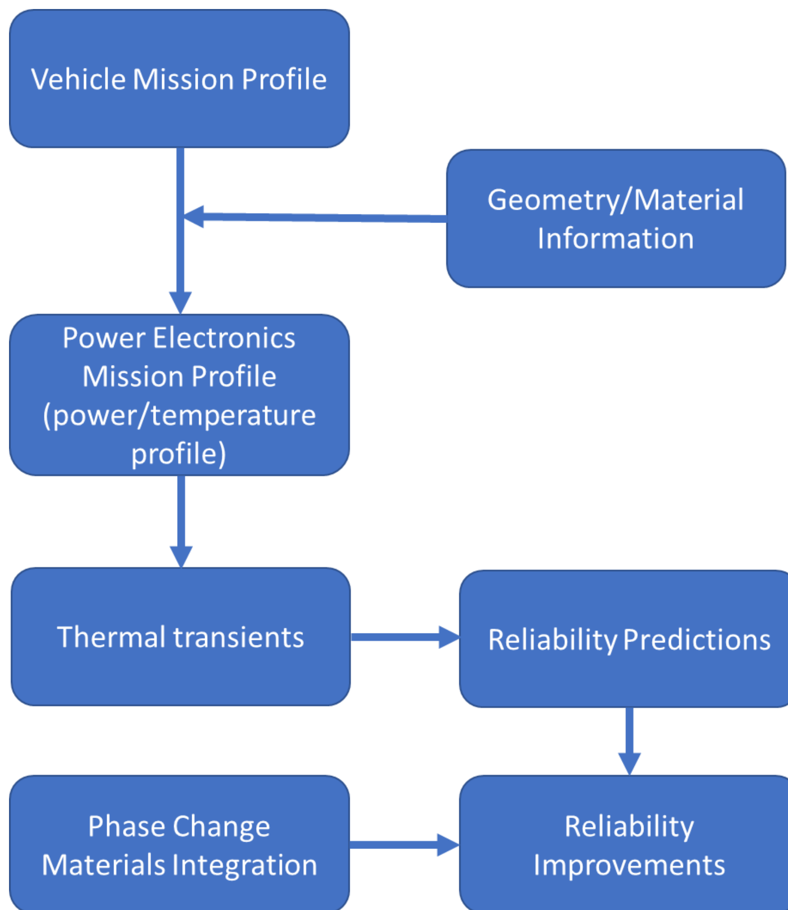

Figure 35. Flow chart summarizing the work presented

A sensitivity study was carried out to see the validity of a data reduction technique in reliability computation. It relied on setting a minimum temperature swing for a mini-cycle to be assumed contributory to cumulative damage. The results obtained are promising, with evidence to suggest that data can be significantly reduced while retaining good stability. For UDDS, 90% stability can

be maintained while reducing number of computations by almost 30%. For HWFET and tractor drive schedule, 90% stable life estimation can be carried out while reducing the number of required computations by 23% and 35%, respectively.

The thermal transients in the power modules are important failure drivers and managing and mitigating them is an important reliability consideration. Phase change materials may offer a promising method of cooling electronics in the context of variable power loads, such as those seen in electric vehicle operation, as they absorb thermal energy while changing phase within a small temperature range and they can also facilitate an extra level of control to the thermal engineer as the PCM works like a constant temperature heat sink. But there is a delicate thermal design optimization that must be considered. Research on PCMs until now have largely focused on consumer electronics, such as mobile devices, but it can bring the same advantages to automotive cooling. Using a computational model to simulate transient temperature distribution, it was shown that using a PCM such as Xylitol can lead to a more consistent temperature profile with lower peaks and smaller temperature swings, under conditions where conduction, convection and latent heat exchange were in the appropriate balance. This in turn can lead to a significant enhancement in useful life of an automotive electronic device. However, the PCM (particularly organic) also increases the thermal resistance from the die to the ambient (or coolant), and thus, for low conductivity PCMs, utility is best at small convection coefficients ($h<10\ W/m^2.K$) and thin PCM layers. Using a medium fidelity fast modeling approach to PCM thermal management design, an expedient operating envelope was presented for xylitol with a typical, commercially available power module as a case study, and it was shown that both peak load and average load will have to be factored in any design decisions, as well as PCM size and cooling method. This work illustrates the importance of design tradeoffs in electronics thermal management, particularly where

automotive power electronics may be concerned; and furthermore, points to the importance of both PCM property enhancement and system integration for realizing passive cooling reliability benefits. Other configurations and materials not considered here may offer greater benefit, but sizing them with the system thermal loads is critical, and thermal designers must consider factors of melt time, re-solidification and material properties in the context of the thermal pulse load and frequency in the design of interest.

The activities presented in this work are summarized in Fig. 35.

6.2 Significance and Future Opportunities

The aim of this work is to address some problems associated with electric and hybrid vehicle operation. There is a dearth of a reliability prediction tool that can provide quick results while also maintaining reasonable fidelity while modeling the thermal transients. There is also the problem of shortened life of drivetrain electronics as a result of the thermal transients.

In order to solve the first problem, this works presents an analytical method to translate the mission profile into reliability estimates, and also discusses a way in which the algorithm can be optimized for computational time while minimizing discrepancy with benchmark. A way to improve the process further would be by taking a more detailed look at the underlying mechanisms. There are significant opportunities here to utilize modern data-driven and machine learning techniques such as principal component analysis to identify the biggest contributors to failure.

As a way of improving electronics reliability by mitigating effects of thermal transients, this work also presented a way to get the best out of phase change materials in automotive electronics cooling. The performance of PCMs was found to be limited by the low thermal conductivity of the PCM materials. This study can be extended to include higher conductivity PCMs, such as nano-

particle enhanced PCMs and metallic PCMs. Successful integration of highly conductive PCMs can significantly widen the scope of PCM integration in heat sinks. Another aspect that requires optimization is effective heat rejection to the environment for faster solidification of PCM. Within the materials widely available, this work has provided a optimization pathway for PCM integration in order to lengthen useful life of drivetrain electronics subject to thermal transients.

Appendix

Appendix A1. Example calculation of motor power from drive schedule

Considered data snapshot:

Time (s)	Speed (mph)	Speed (m/s)
21	3	1.34
22	5.9	2.63

Acceleration = (2.63 – 1.34) / (22 – 21) = 1.29 m/s^2

Force = Mass * Acceleration = 1300*1.29 = 1677 N

Total Tractive Effort (TTE) = Force + Rolling Resistance + Aerodynamic drag + Grade Resistance

where:

Rolling resistance = Coefficient of Rolling Friction * Mass * Gravity

= 0.012 * 1300 * 9.81 = 153 N

Aerodynamic Drag = 0.5 *Air density*Frontal Area*Aerodynamic drag coefficient*speed^2

= 0.5*1.3*2.5*0.6*2.63^2 = 6.74 N

Grade Resistance = 0 N (assuming level surface)

TTE = 1677 + 153 + 6.74 + 0 = 1836.8 N

Required Torque on Drive Wheel = TTE * Friction Factor * Wheel Radius

$= 1836.8 * 1.1 * 0.2 = 404.1$ Nm

Motor Torque = Required Torque on Drive Wheel / Gear Ratio

$= 404.1 / 20 = 20.2$ Nm

Wheel Speed = Speed / (2π*Wheel Radius) = $60 * 2.637 / (2\pi * 0.2) = 125.9$ RPM

Motor Speed = 125.9 * Gear Ratio = 2518 RPM

Motor Power = Motor Torque * 2π * Angular Velocity = 20.2 * 2π * Motor Speed / (60 * 1000) = 5.32 KW

Appendix A2. Thermal and reliability modeling computer program

```
clear

clc



file=input('Please specify temperature profile to open: ','s');

T1=load(file);

len=length(T1);

time = zeros(len,1);

for n=1:len-1

   time(n)= (n-1);

end




T=T1;

T_mean=mean(T);

T_max=max(T);

T_min=min(T);

delta_T=T_max-T_min;
```

```
T_medium=T_min+(0.5*delta_T);

%i=2;

j=1;


for i=2:len-2

    if ((T(i)-T(i-1))*(T(i+1)-T(i)))<0

        a(j)=T(i);

        j=j+1;

    end

end

%a=a';

%i=2;

f=0;  %not frequency, just a counting variable

 for i=2:j-1

     if (abs(a(i)-a(i-1)))>(0.00002*T_mean)

        f=f+0.5;

     end

 end
```

```
frequency=f/(max(time)-min(time));

Tmax_lab=150;

deltaT_lab=100;

T_medium_lab = 100;

frequency_lab=1;

AF_NL=((deltaT_lab/delta_T)^2.65)*((frequency_lab/frequency)^(0.136))*exp(2185*((1/(T_ma
x+273.15))-(1/(Tmax_lab+273.15)))); % exponents for SAC based on Pan et al.


N_NL= exp(9.517 - (2.0635*log(delta_T)) - (0.3452 * log(frequency)) + (2006.4*(1/T_max))); %
exponents for SAC based on Pan et al.


AF_CM=(deltaT_lab/delta_T)^2.7;

fprintf('Solder fatigue AF based on Norris-Landzberg formulation: %f \nSolder fatigue AF based
on Coffin-Manson formulation: %f', AF_NL, AF_CM);

Al_bond_life=(5600000000000000*(delta_T)^(-5.5));

IGBT_life=640*((delta_T)^(-5))*exp(29900/8.314/(T_medium+273.15));

AF_IGBT_life=(((delta_T)^(-5))*exp(29900/8.314/(T_medium+273.15)))/(((deltaT_lab)^(-
5))*exp(29900/8.314/(T_medium_lab+273.15)));
```

```
fprintf('\nIGBT no. of cycles to failure: %f\nAl bond wire no. of cycles to failure: %f\n',IGBT_life,
Al_bond_life);

fprintf('Solder fatigue life based on Norris-Landzberg formulation: %f \n', N_NL);

fprintf('AF life based on Held formulation: %f \n', AF_IGBT_life);
```

Appendix A3. Vitae

Name: Bakhtiyar Mohammad Nafis

Address: 700 Research Center Blvd.

Office 4624

Fayetteville, AR, 72701

Email Address: bmohamma@uark.edu

Education: B.S. Mechanical Engineering, Bangladesh University of Engineering and Technology, 2017